



Fog controls biological cycling of soil phosphorus in the Coastal Cordillera of the Atacama Desert

Sun, Xiaolei; Amelung, Wulf; Klumpp, Erwin; Walk, Janek; Mörchen, Ramona; Böhm, Christoph; Moradi, Ghazal; May, Simon Matthias; Tamburini, Federica; Wang, Ye; Bol, Roland

Global Change Biology

DOI:

[10.1111/gcb.17068](https://doi.org/10.1111/gcb.17068)

Published: 01/01/2024

Publisher's PDF, also known as Version of record

[Cyswllt i'r cyhoeddiad / Link to publication](#)

Dyfyniad o'r fersiwn a gyhoeddwyd / Citation for published version (APA):

Sun, X., Amelung, W., Klumpp, E., Walk, J., Mörchen, R., Böhm, C., Moradi, G., May, S. M., Tamburini, F., Wang, Y., & Bol, R. (2024). Fog controls biological cycling of soil phosphorus in the Coastal Cordillera of the Atacama Desert. *Global Change Biology*, 30(1), e17068. <https://doi.org/10.1111/gcb.17068>

Hawliau Cyffredinol / General rights

Copyright and moral rights for the publications made accessible in the public portal are retained by the authors and/or other copyright owners and it is a condition of accessing publications that users recognise and abide by the legal requirements associated with these rights.












- Users may download and print one copy of any publication from the public portal for the purpose of private study or research.
- You may not further distribute the material or use it for any profit-making activity or commercial gain
- You may freely distribute the URL identifying the publication in the public portal ?

Take down policy

If you believe that this document breaches copyright please contact us providing details, and we will remove access to the work immediately and investigate your claim.

RESEARCH ARTICLE

Fog controls biological cycling of soil phosphorus in the Coastal Cordillera of the Atacama Desert

Xiaolei Sun^{1,2}  | Wulf Amelung^{1,3}  | Erwin Klumpp¹  | Janek Walk⁴  |
 Ramona Mörchen³  | Christoph Böhm⁵  | Ghazal Moradi^{1,2}  | Simon Matthias May⁶  |
 Federica Tamburini⁷  | Ye Wang³  | Roland Bol^{1,8} 

¹Institute of Bio- and Geosciences, Agrosphere (IBG-3), Forschungszentrum Jülich, Jülich, Germany

²Institute for Environmental Research, Biology 5, RWTH Aachen University, Aachen, Germany

³Institute of Crop Science and Resource Conservation (INRES)-Soil Science and Soil Ecology, Rheinische Friedrich-Wilhelms-University Bonn, Bonn, Germany

⁴Department of Geography and Regional Research, University of Vienna, Vienna, Austria

⁵Institute for Geophysics and Meteorology, University of Cologne, Albertus-Magnus-Platz, Cologne, Germany

⁶Institute of Geography, University Cologne, Albertus-Magnus-Platz, Cologne, Germany

⁷Institute of Agricultural Sciences, ETH Zürich, Lindau, Switzerland

⁸School of Natural Sciences, Environment Centre Wales, Bangor University, Bangor, UK

Correspondence

Xiaolei Sun, Institute of Bio- and Geosciences, Agrosphere (IBG-3), Forschungszentrum Jülich, Jülich 52425, Germany.
 Email: xi.sun@fz-juelich.de

Funding information

Deutsche Forschungsgemeinschaft, Grant/Award Number: Projektnummer 268236062-SFB 1211

Abstract

Soils in hyper-arid climates, such as the Chilean Atacama Desert, show indications of past and present forms of life despite extreme water limitations. We hypothesize that fog plays a key role in sustaining life. In particular, we assume that fog water is incorporated into soil nutrient cycles, with the inland limit of fog penetration corresponding to the threshold for biological cycling of soil phosphorus (P). We collected topsoil samples (0–10 cm) from each of 54 subsites, including sites in direct adjacency (<10 cm) and in 1 m distance to plants, along an aridity gradient across the Coastal Cordillera. Satellite-based fog detection revealed that Pacific fog penetrates up to 10 km inland, while inland sites at 10–23 km from the coast rely solely on sporadic rainfall for water supply. To assess biological P cycling we performed sequential P fractionation and determined oxygen isotope of HCl-extractable inorganic P ($\delta^{18}\text{O}_{\text{HCl-P}_i}$). Total P (P_t) concentration exponentially increased from 336 mg kg⁻¹ to a maximum of 1021 mg kg⁻¹ in inland areas ≥ 10 km. With increasing distance from the coast, soil $\delta^{18}\text{O}_{\text{HCl-P}_i}$ values declined exponentially from 16.6‰ to a constant 9.9‰ for locations ≥ 10 km inland. Biological cycling of HCl-P_i near the coast reached a maximum of 76%–100%, which could only be explained by the fact that fog water predominately drives biological P cycling. In inland regions, with minimal rainfall (<5 mm) as single water source, only $24 \pm 14\%$ of HCl-P_i was biologically cycled. We conclude that biological P cycling in the hyper-arid Atacama Desert is not exclusively but mainly mediated by fog, which thus controls apatite dissolution rates and related occurrence and spread of microbial life in this extreme environment.

KEYWORDS

Atacama Desert, fog, hyper-aridity, oxygen isotopes ratio in phosphates, soil P cycle

This is an open access article under the terms of the [Creative Commons Attribution-NonCommercial-NoDerivs](https://creativecommons.org/licenses/by-nc-nd/4.0/) License, which permits use and distribution in any medium, provided the original work is properly cited, the use is non-commercial and no modifications or adaptations are made.

© 2023 The Authors. *Global Change Biology* published by John Wiley & Sons Ltd.

1 | INTRODUCTION

Increasing aridity or even absence of rainfall can be a severe outcome in many regions due to climate change. Currently, global desertification is predicted to rise from 48% to 65% of total land surface in 2035 (González-Pinilla et al., 2021; Lickley & Solomon, 2018; Liu et al., 2020). The increasing aridity threatens the viability of microorganisms, plants and animals and thus their biodiversity (Li et al., 2021; Zhang et al., 2023). However, some organisms are able to survive even in extremely dry environments, like the hyper-arid Atacama Desert, with almost zero rainfall in its inner core zone (Eshel et al., 2021; Schulze-Makuch et al., 2018). Yet, also these forms of life depend on the availability of water. Notably, in such extremely hyper-arid environments essential water can be supplied to the plant–soil system via non-rainfall components like fog (Fuentes, Gómez, et al., 2022; Wang et al., 2022; Zheng et al., 2018). Indeed, fog is known to support ecosystem productivity and functioning in specific coastal environments and montane forests, and its dedicated collection can serve to supply irrigation water in cropping systems (Dawson & Goldsmith, 2018; Fessehaye et al., 2014). It seems therefore reasonable to assume that, especially in hyper-arid ecosystems, fog water may replace rainwater to sustain life.

The Atacama Desert is restricted by the Pacific Ocean in the west and the Andes Cordillera in the east, resulting in three main geologic units, which are the Coastal Cordillera, the Central Depression and the Andes (Evenstar et al., 2017; Voigt et al., 2020; Wang et al., 2014). The special physiographic characteristics coupled with complex ocean–atmosphere processes have generated the extreme hyper-aridity in the Atacama Desert dating back to at least the Miocene (Dunai et al., 2005; Hartley et al., 2005; Sáez et al., 2012). In the south-central Coastal Cordillera, a narrow mountain range exceeding elevations of 3000 m a.s.l., fog plays a dominant role for the humidity (Cereceda et al., 2002, 2008a; Jordan et al., 2015; Moat et al., 2021; Walk et al., 2020). Advective fog results from marine stratocumulus clouds, which is transported by winds to the coast during the night and, there, affects altitudes between 400 and 1200 m a.s.l. with a descending trend of moisture along increasing distance inland (Cáceres et al., 2007; Cereceda et al., 2002; Garreaud et al., 2008; Moat et al., 2021; Schween et al., 2020). For inland regions above 1200 m a.s.l., which are currently lying above the upper fog boundary and therefore cannot be penetrated by fog at present, sporadic rainfall events, which mostly occur during austral winter and are often related to El Niño, are nowadays regarded as the main freshwater source (Azúa-Bustos et al., 2011; Houston, 2006; Ortega et al., 2019; Schulz et al., 2012; Walk et al., 2020). Overall, the Atacama Desert provides a unique habitat to study the adaptation of its ecosystem processes by fog because clear gradients in fog occurrence from the coast into the inland/hinterlands are present.

Along the gradient from the coast towards inland, there is a decreased accumulation of soil soluble salts (Arens et al., 2021; Ewing et al., 2006; Voigt et al., 2020; Wang et al., 2014). Under higher humidity, as present at the coast or further south within the Coastal Cordillera, pedogenic processes such as rubification, silicate

weathering and clay formation were identified (Bernhard et al., 2018; Walk et al., 2023). As has been shown in previous work, this gradient is well represented along a longitudinal transect in the Pajón valley, showing increased accumulation of soil soluble salts and soil organic matter towards the coast (Arens et al., 2021; Mörchen et al., 2019; Voigt et al., 2020). Knief et al. (2020) showed that concentrations of plant-derived and microbiological markers followed this trend, thus giving rise to the assumption that presence of life also leaves a fingerprint on the cycling of nutrients, such as phosphorus (P).

Phosphorus is a crucial and limiting nutrient that plays a vital role in supporting life. Its cycling has a significant impact on key ecosystem services, including primary production and waterbody quality (Helfenstein et al., 2018). Changes in soil P concentrations and bioavailability are mainly driven by geogenic parent minerals (i.e., apatite) and their weathering, with timescales that may extend over millennia (Walker & Syers, 1976; Walton et al., 2023). During the early stages of pedogenesis, P is initially released from apatite to the soil solution and is directly available to plants, which is mirrored by Resin-extractable P. Phosphorus can be subsequently adsorbed by Fe/Al (hydro)oxides or it is taken up and immobilized by microbes and plants. When re-released to the soil solution after cell death and lysis, biologically cycled P can form secondary calcium minerals through re-precipitation. Finally, occluded P forms (Residual-P) can accumulate (Chen et al., 2015; Izquierdo et al., 2013; Walker & Syers, 1976). Similar bio-geochemical P cycling processes are likely to occur along aridity gradients and might affect forms of life in the Atacama Desert (Brucker & Spohn, 2019; Feng et al., 2016; Wilson et al., 2022).

To elucidate P cycling in terrestrial environments, Hedley P fractions are commonly used to identify different P pools based on their different extractability (Hedley et al., 1982). The P extracted by HCl, for instance, largely comprises apatite (Ca-P; Hedley et al., 1982; Roberts et al., 2015). Yet, as soil solution P may also be re-precipitated with Ca, biological P cycling overprints pedogenic precipitation processes (Helfenstein et al., 2018; Reed et al., 2015). Consequently, the use of phosphate oxygen isotope values ($\delta^{18}\text{O}_\text{P}$) has been recommended to evaluate biological processes because the P-O bond can only be broken down through enzymatic processes under the natural soil environments (Gross & Angert, 2015; Shen et al., 2020; Tamburini et al., 2012). Abiotic processes induce little if any oxygen isotope fractionations in phosphate (Jaisi & Blake, 2010). Abiotic oxygen isotope exchange is also lacking in hostile environments like the Atacama Desert characterized by extreme solar UV irradiation and aridity (Shen et al., 2020). Yet, when examining $\delta^{18}\text{O}_\text{P}$ in HCl-extractable soil phosphates ($\delta^{18}\text{O}_\text{HCl-P}$), deviations from the pedogenic apatite value have been found, which then indicate the occurrence of biological processes before precipitation as secondary apatite (Amelung et al., 2015; Helfenstein et al., 2018; Tamburini et al., 2012).

As the concentrations of isotopically altered phosphates in the Atacama Desert exceed concentrations typically found in microbes, Wang, Moradi, et al. (2021) hypothesized that alterations in $\delta^{18}\text{O}_\text{HCl-P}$ values were able not only trace recent but critical past life activities

in this hyper-arid desert. However, Wang, Moradi, et al. (2021) could not directly assign this biological cycling of soil P to specific water sources, because their study area primarily receives during the austral summer convective rainfall originating from the Amazon Basin (Garreaud et al., 2008; Mörchen et al., 2019). The authors could not comprehensively explain the presence of large-scale patterns of biological nutrient cycling across the desert, which likely follow the non-linear gradients in aridity (Bernhard et al., 2018; Brucker & Spohn, 2019; Knief et al., 2020). Yet, for phosphate, an abrupt change in apatite content has been found to occur at a specific threshold of mean annual precipitation (Brucker & Spohn, 2019), making it reasonable to assume that other water sources like fog contributed to such abrupt changes in soil apatite concentration. But how such potential thresholds related to the biological soil P cycling are affected by the presence of fog still warrants clarification.

On a local scale, water availability in the Atacama Desert is heterogeneous, thus promoting patchy plant distribution (Arndt et al., 2020). In the hyper-arid core, only occasional rainfall events can activate geomorphic processes and induce the “blooming desert”, due to the explosive growth and flowering of ephemeral herbaceous and some woody desert species (Chávez et al., 2019; Pfeiffer et al., 2021). Closer to the coast, in turn, additional moisture supply by fog supports the development of fog oases or *loma* vegetation (Figure 1b; Cereceda et al., 2008b; Moat et al., 2021; Mörchen et al., 2021). Plant growth affects the P cycling via increasing apatite dissolution, enhancing organic matter accumulation and promoting the biological cycling of soil P (Brucker & Spohn, 2019; Chávez et al., 2019; Pfeiffer et al., 2021). Nevertheless, our current understanding of the impact of plant growth, particularly in fog ecosystems, on P cycling in the hyper-arid Atacama Desert remains inadequate.

In order to examine whether and to what degree the availability of fog provides ecological thresholds for the biological cycling of P and related survival of soil life, we sampled an east–west trending transect (i.e., the Paposo transect) in the south-central Coastal Cordillera, which has distinct fog-dominated and other solely rain-fed sites. We then assessed both soil Hedley P pools concentration and $\delta^{18}\text{O}_{\text{HCl-P}}$ values. Fog is known to enter the arid region up 400–1200m altitude (Cereceda et al., 2008a, 2008b; Dunai et al., 2020; Garreaud et al., 2008), which in the research area corresponds to a distance of <10 km (Figure 1c). Hence, the aridity increases with distance from the coast along this transect. We hypothesize that (i) fog enables biological cycling of soil P and its importance declines with increasing coastal distance and aridity. (ii) The range of the coastal fog penetration into the desert is a key threshold for biological soil P cycling, while (iii) locally the presence of plant growth enhances the actual biological soil P cycling. As near coastal sites may be affected by additional P input through sea spray primarily attributed to fog penetration (Arenas-Díaz et al., 2022; Cereceda et al., 2002), salt ions were assessed to evaluate related atmospheric dust deposition. The concentration of Na^+ at the soil surface serves as an indicator for sea-salt aerosol (SSA) deposition in the Atacama Desert as Na is not abundant in the parent material and considered inactive in most

of biochemical processes relevant for our study (Li et al., 2019; Wang et al., 2014).

2 | MATERIALS AND METHODS

2.1 | Study area and soil sampling

Soil samples were collected along a west–east transect in the Paposo area (~25°S), ranging in distance to coast and altitude from 2.3 to 22.9 km and 570 to 2110 m a.s.l. (in total of nine sites), respectively (Figure 1, Table S1). The Paposo area is located within the south-central Coastal Cordillera featuring elevations mostly between 500 and 2500 m a.s.l. The north–south extending mountain range presents an uplifted and eroded Mesozoic magmatic arc, composed largely of Jurassic and Cretaceous igneous rocks (Allmendinger & González, 2010; González et al., 2003; Oliveros et al., 2018; Scheuber & González, 1999). The bedrock lithology at all sample sites along the transect consists almost exclusively of plutonic granitoids (Walk et al., 2023). Based on the aridity index (AI; Zomer et al., 2022), the site 2.3 km is located at the arid–hyper-arid transition while all sites further inland are classified as hyper-arid (Figure 1c, Table S1). The mean annual air temperature decreases from 18.0 to 16.7°C (Table S1). Along the transect, a decrease of plant cover from >40% at 3.5 km to <5% beyond 7.6 km can be observed (Mörchen et al., 2021; Table S1), which is concomitant with a decrease in mean annual verdancy of the Loma vegetation, which is assumed to be fog-dependent (Moat et al., 2021; Figure 1b). The most common plants found in the area are *Heliotropium taltalense* I.M. Johnst., *Cristaria integerrima* Phil., *Nolana sedifolia* Kunze ex Walp. and *Huidobria fruticosa* Phil (Mörchen et al., 2021).

Samples were taken in October 2016 and March 2017 (Figure 1; Table S1). A total of six soils were sampled from 0 to 10 cm depth at each site. Three samples were taken near plants in a distance of 0–10 cm (“N” samples). Another three samples were taken far from the plant in a distance ≥ 1 m (“F” samples). All soil samples were air-dried and sieved <2 mm and then transported to Germany. Each sample was homogenized prior to laboratory analyses.

2.2 | Fog occurrence

To acquire long-term fog frequency averages covering our entire study region, we apply the fog retrieval method developed for the Atacama Desert by Böhm et al. (2021). In summary, it exploits satellite observations, that is, spectral radiances, from the Moderate Resolution Imaging Spectroradiometer (MODIS) installed on the Terra and Aqua satellites (Level-1B 1-km Calibrated Radiances Product: MOD021KM, MYD021KM; MODIS Characterization Support Team, 2017a, 2017b). These data products are provided at a 1 km horizontal resolution. To map the spectral radiances to a ground fog state, a neural network was trained with ground-based fog retrievals based on leaf-wetness sensor measurements and other

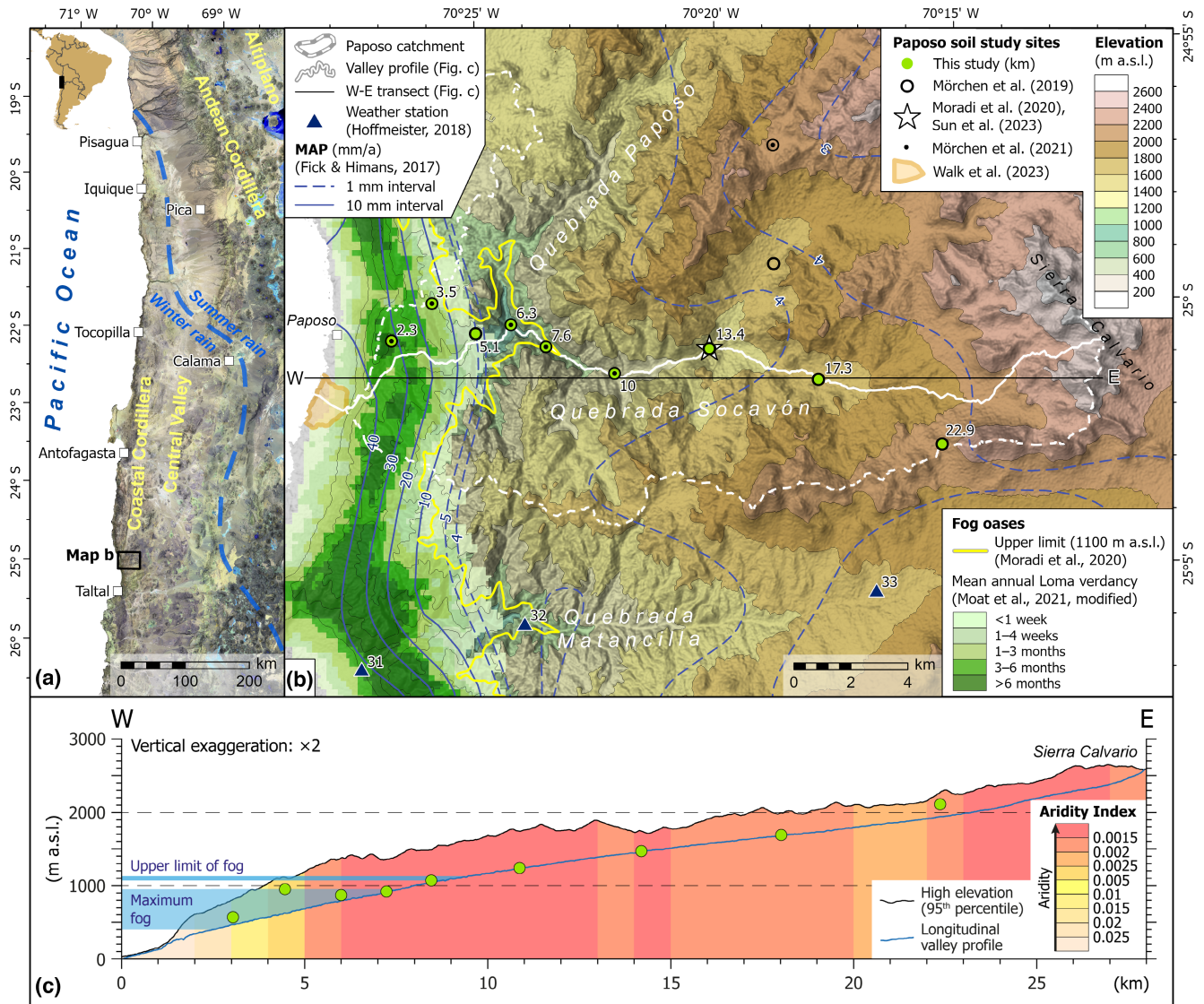


FIGURE 1 (a) Satellite imagery overview map of the Atacama Desert in Northern Chile (USGS Landsat-8 false-colour [SWIR-2/ SWIR-1/NIR] composite of scenes from 23 December 2016 to 21 April 2017); highlighted is the dry diagonal (blue dashed line) after Houston (2006). (b) Relief, precipitation, and vegetation along the Paposo transect in the southern central Atacama Desert; shown are the watershed, the closest CRC 1211 weather stations 31, 32 and 33 (Hoffmeister, 2018), mean annual precipitation (MAP) according to Fick and Hijmans (2017), soil study sites (Sun et al, 2023) investigated in this as well as in previous studies (Moradi et al., 2020; Mörchen et al., 2019, 2021; Walk et al. 2023), the upper limit of fog occurrence according to Moradi et al. (2020), and the mean annual verdancy of Loma vegetation (verdant period over the last 20 years based on the MODIS Normalized Difference Vegetation Index) modified after Moat et al. (2021); elevation data and hillshade: SRTM 1° Global (USGS, 2014). (c) W-E profiles of the high topography and Aridity Index after Zomer et al. (2022) assessed along a 6 km wide swath profile (see central profile line in b) by calculating the 95th percentile of elevation and mean Aridity Index, respectively; further illustrated are the longitudinal valley profile (see course in b), the location and altitude of the PAP study sites (green circles), the upper limit of fog occurrence (Moradi et al., 2020), and the zone of maximum fog occurrence according to Garreaud et al. (2008). Map lines delineate study areas and do not necessarily depict accepted national boundaries.

meteorological data from weather stations deployed throughout the Atacama Desert (Hoffmeister, 2018; Schween et al., 2020). From both satellite platforms, which are in polar orbits, only nocturnal overpass times are considered. Usually, one overpass of each platform is available almost every night for the Atacama Desert region. Specific overpass times range between 22:30 and 00:10 Chile standard time (CLT; Terra) and 01:10 and 02:45 CLT (Aqua) depending on specific orbit characteristics. While the original fog data record only

covered a 3-year period (Böhm et al., 2021), we extended the record to obtain a robust, 19-year long (2003–2021) and seasonally resolved climatology of mean fog frequency for our study region (Figure 2). For the soil sample sites, collocated satellite pixels were identified through nearest-neighbor matching.

In the study region, advective fog from the Pacific Ocean may penetrate far into the zone below 1100 m a.s.l. (Chand et al., 2010; Garreaud et al., 2008; Moradi et al., 2020; Quade et al., 2007),

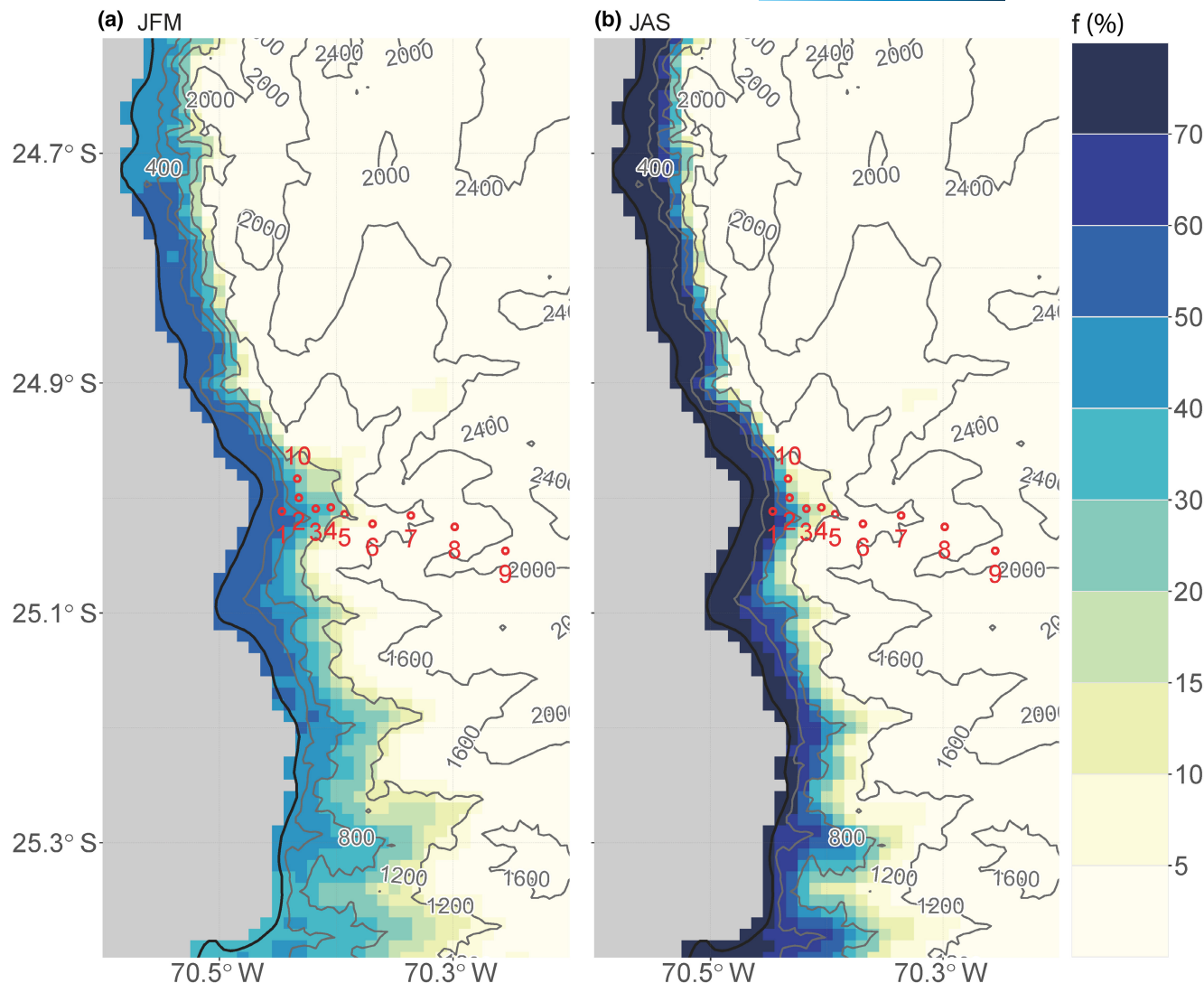


FIGURE 2 Fog occurrence frequency for (a) austral summer (JFM) and (b) winter (JAS) based on the fog retrieval developed by Böhm et al. (2021). Gray contours denote height above sea level every 400 m according to Shuttle Radar Topography Mission data (Farr et al., 2007). Numbered red circles denote the PAP study sites (number 1–9), and the site at 750 m a.s.l. (number 10, 4.3 km from the coast with fog occurrence frequency of 0.21) for which an average fog water flux of $3.36 \text{ mm}^{-2} \text{ day}^{-1}$ at a measuring height above 2 m was reported (Larrain et al., 2002).

reaching around 9–10 km inland along the transect (Figure 1c; Table S1). High fog frequencies exceeding 0.1 are observed for coastal sites 2.3–7.6 km (five sites between 570 and 1070 m a.s.l.) and low values (<0.05) for inland sites 10–22.9 km (4 sites between 1240 and 2110 m a.s.l.; Figures 2 and 6a, Table S1). This indicates that coastal sites are fed by advective fog while inland sites are above the reach of the coastal fog (Cereceda et al., 2008b; Mörchen et al., 2019, 2021).

2.3 | Soil salt ions analysis

The soluble salts were extracted by Milli-Q water at a soil/water ratio of 1:10 (Wang et al., 2017). Then the anions (NO_3^- , Cl^- , and SO_4^{2-}) concentrations in the extracts were analyzed by ion chromatography

(Metrohm IC 850), and those of cations (Ca^{2+} , Na^+ , Mg^{2+} and K^+) were determined by Inductively Coupled Plasma Optical spectroscopy (ICP-OES, iCAP 6500). Sodium Adsorption Ratio (SAR) was used as an index for soil salinity and sodicity, which was calculated by the following formula (Farhangi-Abriz & Ghassemi-Golezani, 2021):

$$\text{SAR} = \frac{\text{Na}^+}{\sqrt{1/2(\text{Ca}^{2+} + \text{Mg}^{2+})}} \quad (1)$$

The SAR exceeded the critical value of 13, classifying the soils as sodic (Bischoff et al., 2018). High salinity provokes microbial activities of some halophyte species and starts to hamper overall microbial P cycling. In fact, the indigenous microorganisms are found to be challenged by the increasing osmotic stress with higher sodicity (Boy et al., 2022; Farhangi-Abriz & Ghassemi-Golezani, 2021;

Fuentes, Choque, et al., 2022; Shen et al., 2021). Furthermore, the higher SAR can be attributed to the enrichment of Na^+ , which originates from sea spray, erosion of inland *playas* and Salars, as well as anthropogenic factors like automobile exhaust or mining. The Coastal Cordillera serves as a barrier that hinders the input of material from the Central Valley into the Pajoso transect. Voigt et al. (2020) argues that strip mining of for example, thenardite (Na_2SO_4) emitted large quantities of dust and may thus be a cause for elevated Na^+ in the inland. A very high SAR indicates that the site should be considered an outlier in the study of biogeochemical processes due to both sodicity and possible anthropogenic impacts.

2.4 | Soil sequential P fraction

Sequential P fractionation was performed according to the Hedley sequential fractionation scheme as modified by Tiessen and Moir (1993). In brief, 0.5 g of each air-dried soil sample was sequentially extracted with four reagents including (i) 30 mL deionized water with two anion exchange resin stripes; (ii) 30 mL 0.5 M NaHCO_3 solution at pH 8.5; (iii) 30 mL 0.1 M NaOH; and (iv) 25 mL 1 M HCl. Finally, *aqua regia* was used at 130°C to extract residual P as chemically most stable P form. After fractionation, the concentration of inorganic P (P_i) in the extracted solutions was measured by the molybdenum blue colorimetric method and measured at 890 nm by the Photometer Analytik Jena SPECORD 205. Total P (P_t) was measured by ICP-OES (ICAP 6500), and the difference between P_t and P_i was used as organic P (P_o).

2.5 | Oxygen isotope composition of HCl-extractable P_i

For analysis of the oxygen isotope values of HCl-extractable P_i ($\delta^{18}\text{O}_{\text{HCl-P}_i}$), we followed the method presented by Tamburini et al. (2010), which produced organic matter-free silver phosphate (Ag_3PO_4) from acid extracts for oxygen analysis. Twenty grams air-dried soils were successively extracted by 0.5 M NaHCO_3 , 0.1 M NaOH and 1 M HCl at a 1/10 soil/solution ratio (Amelung et al., 2015). We discarded the alkaline extracts to remove most of the organic P compounds and polyphosphates, so that only the 1 M HCl extract was used for further purification process. The phosphate was precipitated as ammonium phosphomolybdate and magnesium ammonium phosphate successively. Cation exchange resin (Dowex 50X8, 200–400 mesh, Sigma-Aldrich, Darmstadt, Germany) was used to extract all cations from the solutions and finally precipitated as silver phosphate (Ag_3PO_4). The Ag_3PO_4 crystals were dried in an oven at 50°C for a few days and yellow euhedral Ag_3PO_4 crystals formed after 1 or 2 days.

The $\delta^{18}\text{O}$ value of Ag_3PO_4 was measured at the Plant Nutrition group at ETH Zurich. Each sample was analyzed in duplicates (resulting in a total of $n=108$) using a Vario PYRO Cube (Elemental,

Hanau, Germany) with a C-based reactor coupled in continuous flow to an Isoprime 100 isotope ratio mass spectrometer (Isoprime, Manchester, UK). The furnace was kept at 1450°C and the produced reaction gases were concentrated by a purge and trap chromatography system. Calibration was performed against an internal Ag_3PO_4 standard ($\delta^{18}\text{O}=14.1\text{‰}$) and two international benzoic acid standards (International Atomic Energy Agency; IAEA 601, $\delta^{18}\text{O}=23.1\pm 0.5\text{‰}$ and IAEA 602, $\delta^{18}\text{O}=72.2\pm 0.5\text{‰}$). All values were reported in the conventional delta notation relative to Vienna Standard Mean Oceanic Water (VSMOW) after calibration.

2.6 | Estimation of the equilibrium range of $\delta^{18}\text{O}_p$

The theoretical equilibrium range of $\delta^{18}\text{O}_p$ was calculated based on the empirical equation made by Chang and Blake (2015), which shows the complete equilibration of oxygen isotopes between phosphate with ambient water mediated by pyrophosphatase enzymes:

$$\delta^{18}\text{O}_p = e^{\left(\frac{14.43}{T} - \frac{26.54}{1000}\right)} \times (\delta^{18}\text{O}_w + 1000) - 1000, \quad (2)$$

where T is the ambient soil temperature in (K) and $\delta^{18}\text{O}_p$ and $\delta^{18}\text{O}_w$ are $\delta^{18}\text{O}$ values of phosphate and ambient water in (‰), respectively. Long-term T was needed to calculate the equilibrated values because of the long turn-over time for the HCl-P fraction (Angert et al., 2012; Bauke et al., 2022). Data from three weather stations around ~10 km to the south of the study transect (Nr. 31 at 25°06'54.3" S, 70°27'28.7" W, 160 m a.s.l.; Nr. 32 at 25°06'03.6" S, 70°24'03.6" W, 1011 m a.s.l.; and Nr. 33 at 25°05'29.7" S, 70°16'42.9" W, 1746 m a.s.l.) were used to estimate the soil temperature (Figure 1b; Dunai et al., 2020; Hoffmeister, 2018). Soil temperature was collected from surface to ~10 cm for nearly 4 years (2018–2022). Though these stations records were not prolonged to 20 years or more as in other studies (Bauke et al., 2022; Wang, Moradi, et al., 2021), they still provide robust climatic data for the estimation of equilibrium oxygen isotope fractionations in phosphate (Wang, Bauke, et al., 2021). The average soil surface temperature (0–10 cm) monitored by the weather stations was $21\pm 0.4^\circ\text{C}$. A 0.4°C fluctuation leads to a mere 0.07‰ shift of the calculated range and accounts for less than 0.7% of the biological P cycling process. Thus, 21°C was used as the average soil temperature along the Pajoso transect.

Water sources for near-surface soil life in the Atacama Desert potentially originate from occasional rainfall, fog penetration, and gypsum hydration water (Cereceda et al., 2008b; Palacio et al., 2014; Shen et al., 2020). Rainwater and fog are considered the dominant soil water sources along the Pajoso transect as no surface crusts and gypsic subsurface horizons were detected at lower altitudes between 900 and 1200 m a.s.l. (Voigt et al., 2020). In order to calculate equilibrium $\delta^{18}\text{O}$ values of phosphate within potential uncertainties, we have to consider minimum and maximum in $\delta^{18}\text{O}$ values of the rain and fog water, respectively. The $\delta^{18}\text{O}$ value of rainfall ($\delta^{18}\text{O}_r$) is considered constant below 2500 m along the Pajoso transect (Aravena et al., 1989; Quade et al., 2007), although at higher

elevations the ^{18}O of rainfall is usually depleted (Aravena et al., 1999; Boschetti et al., 2019; Jordan et al., 2019). Based on the limited variation detected in the $\delta^{18}\text{O}$ value of rainfall ($\delta^{18}\text{O}_R$, $-5.6 \pm 0.7\%$) and fog ($\delta^{18}\text{O}_F$, $-1.9 \pm 0.7\%$; Aravena et al., 1989), we used -5.6% and -1.9% as the minimum $\delta^{18}\text{O}_R$ and $\delta^{18}\text{O}_F$, respectively. To estimate maximum $\delta^{18}\text{O}$ values of water sources, we consider that strong, long-term evaporation usually enrich heavy stable isotopes in soil water (Cappa et al., 2003; Rothfuss et al., 2015), which may account for $+6\%$ as upper limit of rainfall equilibrium range for soil phosphates (Wang, Moradi, et al., 2021). Therefore, $+0.4\%$ (-5.6% plus 6%) was taken as upper limit of $\delta^{18}\text{O}_R$ and $+4.1\%$ (-1.9% plus 6%) was the maximum $\delta^{18}\text{O}_F$ after considering evaporation effects. The equilibrium range of $\delta^{18}\text{O}_P$ values therefore corresponded to 20.5–26.6‰ for fog and 16.7–22.8‰ for rainfall, respectively.

2.7 | Contribution of biological P cycling in HCl-extractable P_i

The P fraction that is biologically turned-over in the Paposo region of the Atacama was calculated similarly to the equation used in the Aroma region of the Atacama before (Gross & Angert, 2015; Wang, Moradi, et al., 2021):

$$P_{\text{(contribution by biological cycling)}} = \frac{\delta^{18}\text{O}_{P(\text{HCl-P})} - \delta^{18}\text{O}_{P(\text{parent materials})}}{\delta^{18}\text{O}_{P(\text{equilibrium})} - \delta^{18}\text{O}_{P(\text{parent materials})}} \times 100, \quad (3)$$

where $\delta^{18}\text{O}_{P(\text{parent materials})}$ is the $\delta^{18}\text{O}_P$ values of the parent material, $\delta^{18}\text{O}_{P(\text{HCl-P})}$ is the $\delta^{18}\text{O}_P$ values of the soil HCl-P pool, and $\delta^{18}\text{O}_{P(\text{equilibrium})}$ is the isotopic equilibrium value. The parent material, igneous rocks of the Matancilla plutonic complex (Álvarez et al., 2016; Escribano et al., 2013), can be considered as a result of high temperature formation mechanism (Smith et al., 2021) and, thus, as sufficiently homogeneous along the transect in regards to its $\delta^{18}\text{O}_P$ signature. Igneous rocks typically feature relatively low $\delta^{18}\text{O}_P$ signatures. The $\delta^{18}\text{O}_P$ values of apatite in igneous rock is reported to be 6–8‰ (Blake et al., 2010). This is an agreement with a parent material-rich sample from the site at 13.7 km (1470 m a.s.l.) obtained from 55 to 65 cm depth (6.08‰; Moradi, 2023). We therefore set the value $\delta^{18}\text{O}_P$ values of apatite as 6‰ for our study sites.

2.8 | Statistical evaluation

Analyses of variance (ANOVA) and Post Hoc tests were performed using spss v22.0 (IBM, USA) to assess the effects of distance from the coast and plant distribution on the concentration of salt ions, SAR, soil Hedley P concentrations and $\delta^{18}\text{O}_P$ values in the surface soil (0–10 cm). The significance of differences was determined by the Tukey test. Pearson correlations were used to detect the relationships between $\delta^{18}\text{O}$ of HCl-extractable P_i ($\delta^{18}\text{O}_{\text{HCl-P}_i}$) with HCl- P_i and the fog occurrence frequency. As best fit for the non-linear change in Hedley P concentrations (P_t and P_o), the contribution of

HCl-P to the P_i and P_o pools, and $\delta^{18}\text{O}_{\text{HCl-P}_i}$, we used a mono-exponential regression model:

$$Y(d) = A \times e^{-kd} + Y_e, \quad (4)$$

where $Y(d)$ is the parameter of issue at distance from the coast d (km), A is a rate constant, Y_e is the parameter at absolute equilibrium, and k is a rate constant. Change rates were determined using the first derivative of (4) as:

$$Y'(d) = A \times k \times e^{-kd} \quad (5)$$

Y_e in our calculation was defined as unit-distance increase ($Y'(d) < 0.1\%$ of absolute value of the respective parameter. Figures were constructed using the OriginPro v9.1 software (OriginLab, USA).

3 | RESULTS

3.1 | Salt ions analysis

The soils collected far from the plants were generally saline with SAR values averaging 17.6 mmol L^{-1} , which was larger than the upper limit for soil salinity (13 mmol L^{-1} ; Figure 3a). Correspondingly, even when plants were present at the sites, soils allocated 13.4 km and more away from the coast could be classified as saline (Figure 3a). We consider the site 17.3 km from the coast (1690 m a.s.l.) as an outlier based on its excessive SAR value (33.2 mmol L^{-1}), which was twice the salinity threshold value (26 mmol L^{-1}). It was therefore excluded from subsequent ANOVA analysis of the salt content and other parameters (e.g., Hedley P concentrations and phosphate ^{18}O ; Figure 3a).

Salt ion (Na^+ , K^+ , Mg^{2+} , Cl^- , and NO_3^-) contents were significantly influenced by the distance to coast and the presence of plants, while no variations of Ca^{2+} and SO_4^{2-} were detected among sites (Tables S2 and S4). The concentration of Na^+ in soils far away from the plants tended to decrease with the distance away from the coast. The site near the ocean, 2.3 km away from coast, showed significantly higher Na^+ concentration compared to the sites 5.1 km and site 13.4 km (Figure 3b, Table S2).

3.2 | P pools extracted by sequential P fractionation

The P_t extracted by Hedley accumulated significantly with increasing distance to the coast, ranging from $324 \pm 35 \text{ mg kg}^{-1}$ in 2.3 km distance to the coast to $752 \pm 130 \text{ mg kg}^{-1}$ at a distance of 22.9 km (Figure 4, Table S3). P_i concentrations increased along this direction, while soil P_o concentrations fluctuated with increasing distance to the coast (Figure 4). The maximum P_o concentration was detected 13.4 km away from the coast, with $370 \pm 69 \text{ mg P}_o \text{ kg}^{-1}$ soil, while the lowest P_o concentration was $46 \pm 31 \text{ mg kg}^{-1}$ measured at the site 22.9 km away from coast. The HCl-P was the dominant P pool. It comprised $79 \pm 15\%$ of the overall Hedley-P at sites from 3.5 to

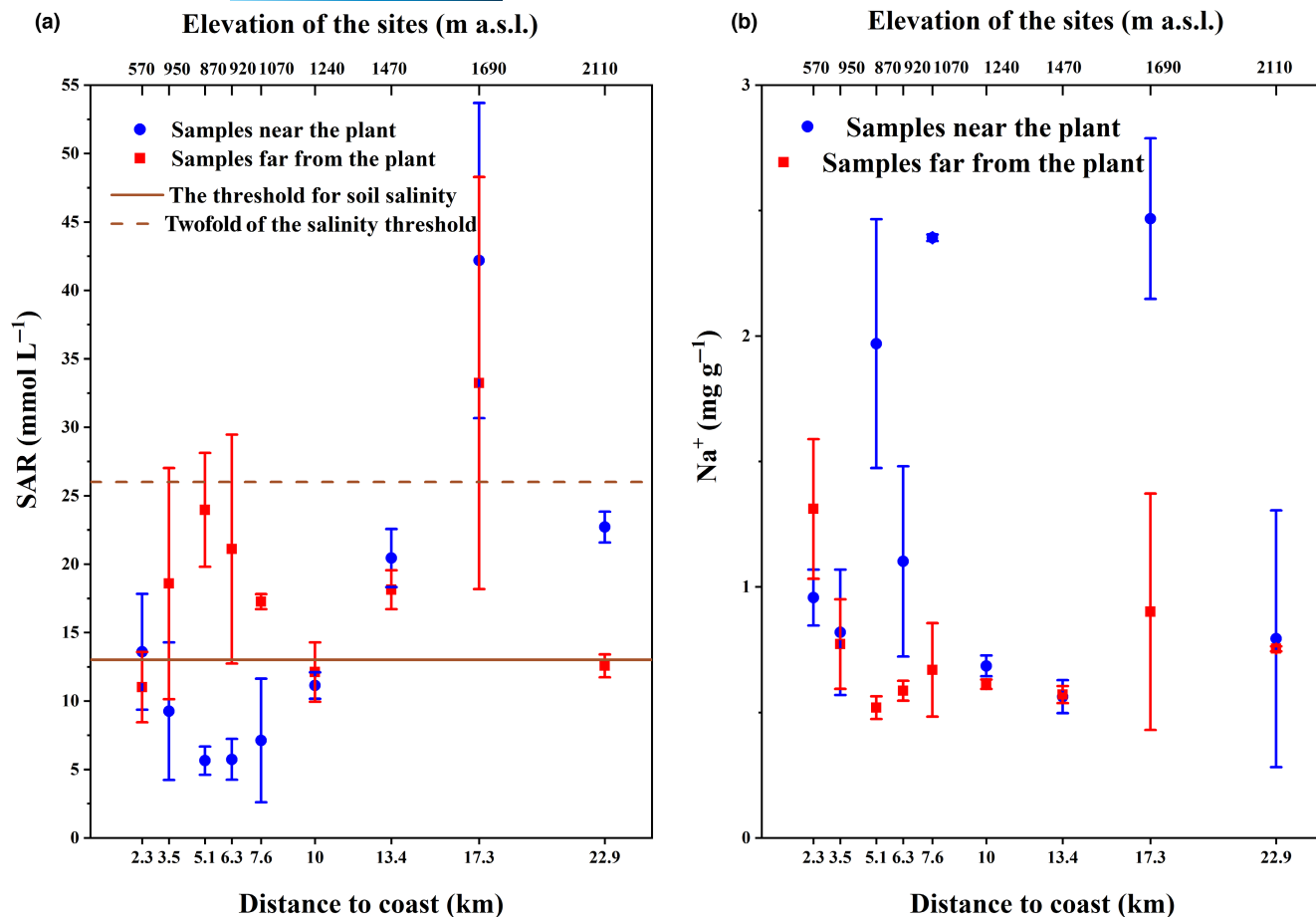


FIGURE 3 The ratio of SAR (a) and the concentration of Na⁺ (b) in surface soil samples along the distance to coast in Paposo. The solid line in (a) is the threshold for soil salinity (13; Farhangi-Abri & Ghassemi-Golezani, 2021). The dot line in (a) represents the twofold of the salinity threshold (26). The data from three subsites at given fog abundance were pooled, and the error bars represent the standard deviation of the mean ($n=3$).

22.9 km away from the coast (Figure 4, Table S3). Only in the proximity to the coast (2.3 km), residual P extracted by *aqua regia* was the predominant P pool ($41 \pm 6.5\%$ of all P forms found), while the HCl-P accounted only for $34.5 \pm 7\%$.

Noteworthy, both HCl-P_i and -P_o increased significantly with increasing distance to coast, while the more easily extractable P and NaOH-extractable pools showed a declining trend (Figure 5). The accumulation of P_i and the increasing contribution of HCl-P pools could be described with mono-exponential rises to a constant maximum (Figures 4 and 5). The calculation showed that for the four P parameters (the P_t concentrations, the P_i concentrations, and the contribution of HCl-P to the P_i and P_o pools), a relatively steady-state equilibria (with P_t concentration of 1021 mg kg^{-1} , P_i concentration of 779 mg kg^{-1} , 99% of P_i and 94% of P_o) would have been attained at distances exceeding 10 km from the coast (Table 2).

The presence of plant affected the concentrations of resin-P, NaOH-P_o and residual-P significantly ($p < .05$), but there were no significant effects on any other P fraction ($p > .05$; Table S5). In general, plant growth enhanced soil resin-P concentrations at the expense of lower NaOH-P_o and residual-P, with effects on HCl-P not being detected (Table S3).

3.3 | Oxygen isotope composition of HCl-extractable P_i ($\delta^{18}\text{O}_{\text{HCl-P}_i}$)

The oxygen isotope values of HCl-extractable P_i ($\delta^{18}\text{O}_{\text{HCl-P}_i}$) values varied from 7.9 to 17.8‰ (Table S3). Only the $\delta^{18}\text{O}_{\text{HCl-P}_i}$ value of the samples taken far away from plants at site 2.3 km was in the range of the calculated equilibrium of rainfall but below that estimated for fog, which however provided the main water source at this point (Figure 6b). At all other sites, the $\delta^{18}\text{O}_{\text{HCl-P}_i}$ values were below the equilibrium range estimated for the minimum and maximum isotope values both for fog or rainfall. Moreover, a decline in $\delta^{18}\text{O}_{\text{HCl-P}_i}$ values was observed with the increasing distance from the coast (Figure 6b). It also followed a mono-exponential fitting curve until a relatively steady state value of 9.9‰ was reached for site distances beyond 10 km from the coast (Table 2, Figure 6b). However, the fitted $\delta^{18}\text{O}_{\text{HCl-P}_i}$ values changed rapidly within the near coastal section of the transect (2.3–10 km) from approximately 16.6–9.9‰ (Table 2, Figure 6b). The related contribution of biological P cycling to total P therefore followed a similar pattern. The highest proportions of biologically cycled P were found near the coast, reaching a maximum of 76% with fog as sole water source

FIGURE 4 Concentration of different P pools extracted by sequential Hedley P fractionation method (mg kg^{-1}) plotted against the distance to the coast at Paposo. N and F represent the samples taken near the plant (0–10 cm) and far from the plant (>1 m), respectively. Data from three subsites at given fog abundance were pooled, and the error bars indicate the standard deviation of the mean ($n=3$). The content in (a) represents the inorganic P pool (P_i) extracted following the Hedley fractionation and the black solid line in (a) is the mono-exponential regression line between Hedley inorganic P content and the distance to the coast without the site 17.3 km. The asterisks indicate level of significance: * $p < .05$, ** $p < .01$, *** $p < .001$. The content in (b) is the organic P pool + Residual P pool.

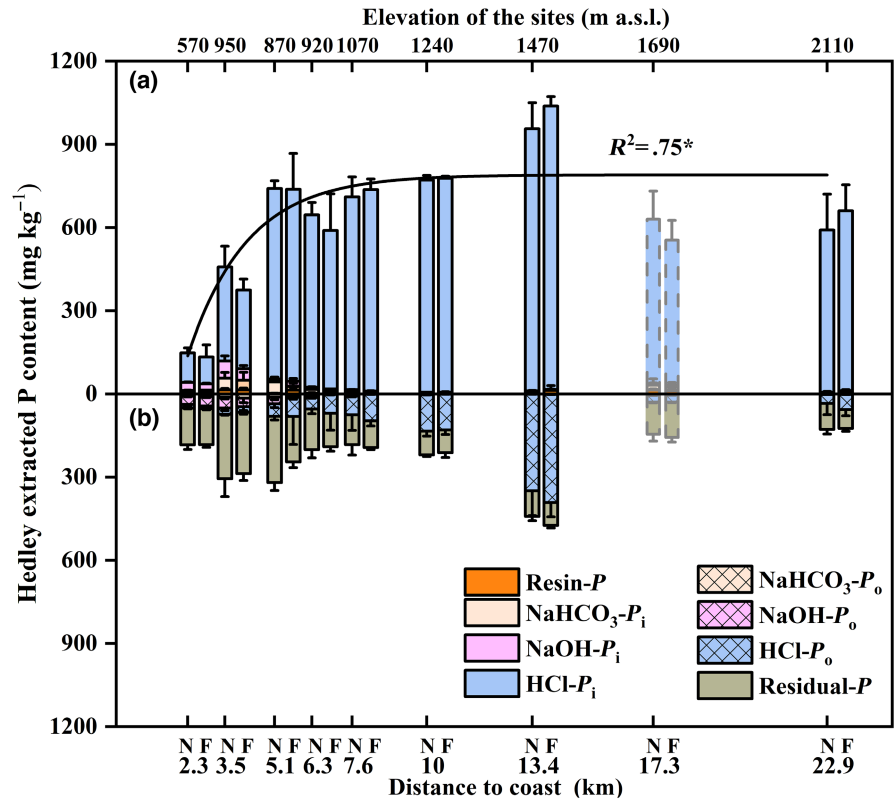
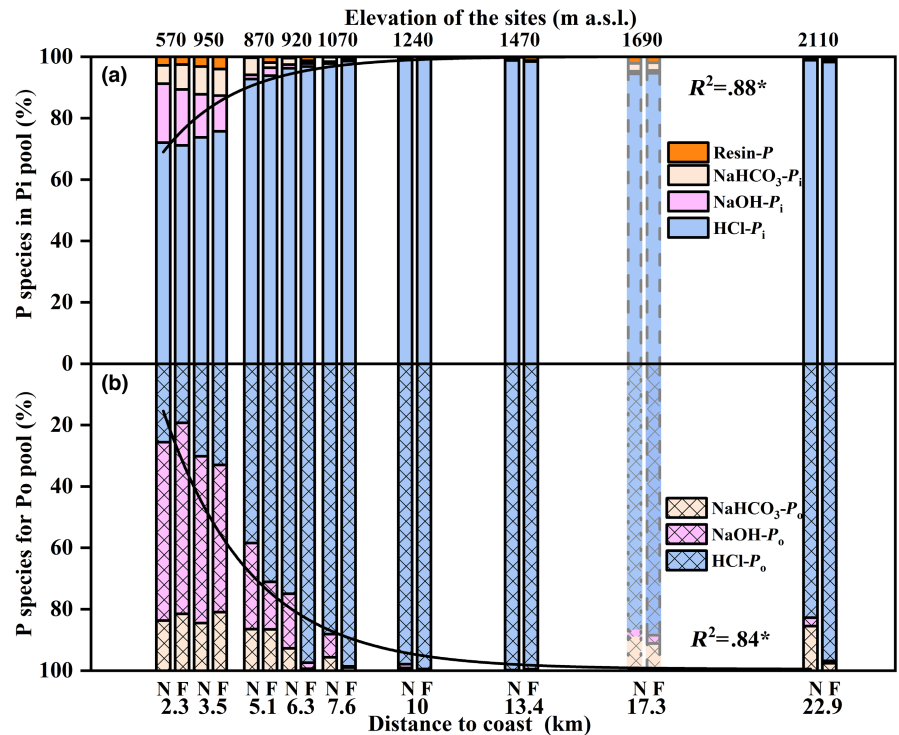


FIGURE 5 (a) The proportion of different P species for Hedley-extractable inorganic phosphorus and (b) the proportion of different P species for Hedley extracted organic phosphorus (P_o) plotted against the distance to the coast at Paposo. Data from three subsites at given fog abundance were pooled, and the error bars represent the SD of the mean ($n=3$). N and F represent the samples taken near the plant (0–10 cm) and far from the plant (>1 m), respectively. The black solid line represents in (a) the mono-exponential regression line between HCl-extracted P_i /Hedley P_i and the distance to the coast and in (b) the mono-exponential regression line between HCl-extracted P_o /Hedley P_o and the distance to coast; for both cases neglecting the site 17.3 km. The asterisks indicate level of significance: * $p < .05$, ** $p < .01$, *** $p < .001$.



used for the calculation but exceeding 100% if rainwater was the only water source (Table 1). At least the maximum values can thus only be explained when accepting fog as additional water source, which is also likely, given high fog frequency near the coast with potential large water yields in fog collectors (Figure 6a; Figure S1). Lower contributions of microbial cycled P were calculated for the section 10–22.9 km of the transect, comprising 21%–33% of total

P (outlier site 17.3 km away from coast excluded; Table 1). We failed to detect an influence of the plants on soil surface $\delta^{18}\text{O}_p$ values ($p < .05$; Table S5).

A linear relationship was found between $\delta^{18}\text{O}_{\text{HCl-P}_i}$ and HCl- P_i concentrations ($p < .001$; Figure 7a). In addition, our analysis showed that $\delta^{18}\text{O}_{\text{HCl-P}_i}$ values were significantly correlated with fog occurrence frequency ($p < .001$; Figure 7b).

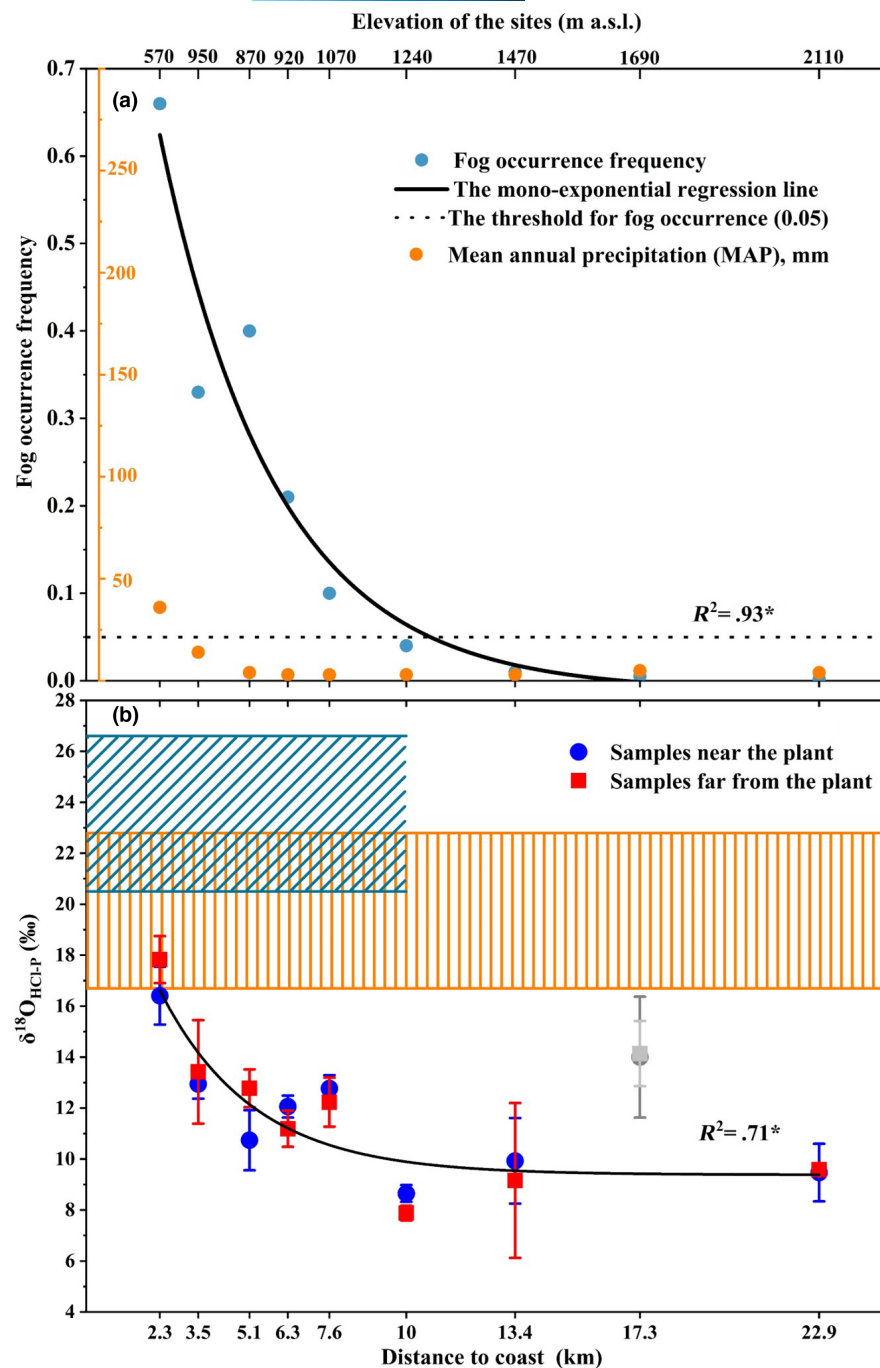


FIGURE 6 (a) The fog occurrence frequency and mean annual precipitation (mm) at the studied sites along the Paposo transect. The black line is the mono-exponential regression line between fog occurrence frequency with distance to the coast. (b) $\delta^{18}\text{O}$ of HCl-extractable P_i ($\delta^{18}\text{O}_{\text{HCl-P}_i}$) values at the surface soils (0–10 cm) along the distance to coast in Paposo. The orange area with vertical lines shows the equilibrium range of $\delta^{18}\text{O}_{\text{HCl-P}}$ calculated based on the $\delta^{18}\text{O}$ of rainfall ($\delta^{18}\text{O}_R$). The turquoise area with slant lines represents the equilibrium range of $\delta^{18}\text{O}_{\text{HCl-P}_i}$ calculated by the $\delta^{18}\text{O}$ of fog ($\delta^{18}\text{O}_F$), which only applies to the sites affected by coastal fog (<1200 m a.s.l.). The black line is the mono-exponential regression line between $\delta^{18}\text{O}_{\text{HCl-P}_i}$ and the distance to the coast without the site 17.3 km. Data from three subsites at given fog abundance were pooled, and the error bars represent the SD of the mean ($n=3$). The asterisk indicates level of significance: * $p < .05$, ** $p < .01$, *** $p < .001$.

4 | DISCUSSION

4.1 | The biogeochemical P transformation with distance to coast

The Na^+ contents showed no significant site variations from 3.5 to 22.9 km distance to coast (Tables S2 and S4), indicating that a clear consistent gradient in sea spray deposition was absent along the transect. Only the near the coast Na^+ portions exceeded that of two inland sites (5.1 and 13.4 km), which may point to some elevated sea spray influence (Figure 3b). However, considering that aerosol concentrations of total P is $2 \text{ ng m}^{-2} \text{ a}^{-1}$ from the Pacific Ocean (Vet

et al., 2014), and assuming that this concentration remains typical for the Atacama Desert region as well, a 1.85-fold difference in sea spray deposition would add 2 mg P m^{-2} over 1 million years at site 2.3 km and 1.08 mg P m^{-2} per million years at inland sites. This difference is insufficient to explain differences in P contents across the sites (Figure 4) or to affect plant productivity. Hence, we discount sea spray deposition as main driver for differences in soil P pools, but rather attribute the latter to the differential biogeochemical transformations of parent material.

The HCl-extractable P pool, which is interpreted as Ca-P (Brucker & Spohn, 2019; Roberts et al., 2015), was the dominant P pool at all sites except for the one nearby the coast (2.3 km

TABLE 1 The percentage of biologically cycled P in HCl-Pi pool.

Distance to coast (km)	Biologically cycled P equilibrated with fog (%)			Biologically cycled P equilibrated with rainfall (%)		
	Min	Mean	Max	Min	Mean	Max
2.3	54±6 ^a	65±14	76±8	66±7	83±22	104±11
3.5	35±7	42±11	50±9	43±8	55±16	67±13
5.1	28±7	34±10	40±10	34±8	44±15	54±13
6.3	27±3	33±7	39±5	33±4	43±11	53±7
7.6	32±4	38±8	45±6	39±4	50±13	61±7
10	—	—	—	14±3	17±6	21±5
13.4	—	—	—	21±13	27±18	33±21
17.3	—	—	—	47±10	62±19	75±16
22.9	—	—	—	21±4	27±8	33±7

^aThe value was given as mean±SD.

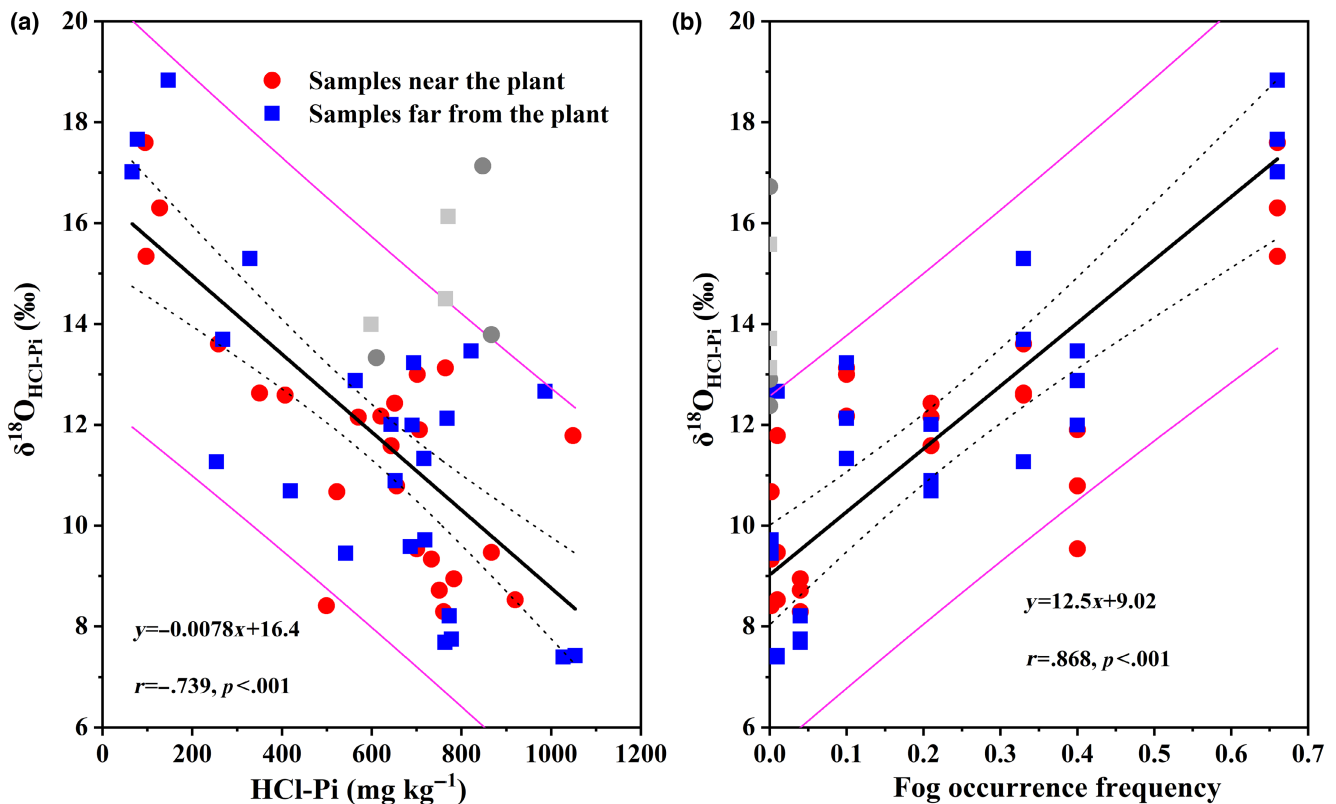


FIGURE 7 (a) Correlation analysis between $\delta^{18}\text{O}$ of HCl-extractable P_i ($\delta^{18}\text{O}_{\text{HCl-P}_i}$) with HCl-P_i without the site 17.3 km. (b) Correlation analysis between $\delta^{18}\text{O}$ of HCl-extractable P_i ($\delta^{18}\text{O}_{\text{HCl-P}_i}$) with fog occurrence frequency without the site 17.3 km.

distance; Figure 4, Table S3). Likely, this reflects the impact of soil moisture on apatite dissolution, since the proportion of Ca-P increased gradually along the transect up to $87.4 \pm 3.9\%$ at the site 22.9 km (Figure 4, Table S3). Concordantly, Shen et al. (2020) reported that Ca-P was less at arid sites, with 55% of the P_t value compared to 75% at hyper-arid sites. The concomitant increase in other P pools such as labile P (Resin-extractable P + NaHCO_3 -extractable P) and Fe/Al bound-P (NaOH-extractable-P) with decreasing portions of Ca-P (Figures 4 and 5, Table S3) therewith reflects that apatite dissolution releases available P. These results

agree with observations from chronosequences (Selmants & Hart, 2010; Turner & Condon, 2013; Walker & Syers, 1976) and climosequence models in dry ecosystems (Bernhard et al., 2018; Brucker & Spohn, 2019; Feng et al., 2016), which pointed out that P in primary minerals depletes over time until new steady-state conditions are reached at improved water availability, equated with retrogression (Gallardo et al., 2020). It should be noted, though, that here we faced two different main water sources, with fog additionally contributing to soil moisture and weathering of P bearing minerals closer to the coast. Beside variations in

TABLE 2 Kinetic parameters of the mono-exponential model (Equation 4: $Y(d) = A \times e^{-kt} + Y_e$) calculated for Hedley P concentrations (P_t and P_i), the contribution of HCl-P to the P_t and P_o pools and $\delta^{18}\text{O}$ of HCl-extractable P_i (see also curve fits in Figures 4–6).

Parameter	Unit	k	A	Y_e	$Y_{2.3}$	$Y_{3.5}$	$Y_{5.1}$	$Y_{6.3}$	$Y_{7.6}$	Y_{10}	$Y_{13.4}$	$Y_{22.9}$	Distance to steady-state ^a (km)	R^{2b}
P_t concentrations	mg kg^{-1}	0.62	-2855	1027	336	697	904	968	1001	1021	1026	1027	15.9	.51*
P_i concentrations	mg kg^{-1}	0.53	-2184	790	137	442	640	710	750	779	788	790	17.8	.75*
HCl-P/ P_t	%	0.42	-82	100	69	81	91	94	97	99	100	100	13.9	.88*
HCl- P_o / P_o	%	0.36	-191	99.2	15	45	69	79	87	94	98	99	18.3	.84*
$\delta^{18}\text{O}_{\text{HCl-P}_i}$	‰	0.34	16	9.7	16.6	14.2	12.1	11.2	10.6	9.9	9.5	9.4	11.7	.64*

Abbreviations: k, A, rate constant; Y_e , equilibrium value; $Y_{2.3}$, $Y_{3.5}$, $Y_{5.1}$, $Y_{6.3}$, $Y_{7.6}$, Y_{10} , $Y_{13.4}$, $Y_{22.9}$, fitted values at varied distance away from the coast, respectively.

^aDefined as unit-distance increase <0.1 of absolute value of the respective parameter.

^bCoefficient of determination of the curve fits (see Figures 4–6), asterisks indicate level of significance: * $p < .005$, ** $p < .01$, *** $p < .0001$; mono-exponential regression.

palaeoprecipitation, also the altitudinal and thus spatial distribution of fog is considered to have varied throughout the past in the coastal Atacama, closely coupled to changes in sea surface temperature as well as sea level (Walk et al., 2022).

With increased biological P consumption, earlier climosequence studies suggested that the contents of organic P (P_o) gradually increased with improvements in water supply (Brucker & Spohn, 2019; Feng et al., 2016; Margalef et al., 2021). Also, additional residues of plants and microorganisms have been detected along the transect with increasing humidity (Knief et al., 2020; Margalef et al., 2021; Mörchen et al., 2019). Inconsistently, our results, show that P_o fluctuated across the soil climosequence with the largest P_o pool being detected in the hyper-arid inland (13.4 km away from coast, 1470 m a.s.l.; Figure 4b, Tables S1, S3 and S5), which coincides with an alluvial fan formed by past extreme rainfalls events in this otherwise hyper-arid climate (Moradi et al., 2020). Likely, microbes and plants utilized some of the available P from the soil by re-mineralizing it from organic forms (Bünemann, 2015; Hinsinger, 2001; Weihrach & Opp, 2018). Therefore, the accumulation of P_o is dependent both on biological productivity and mineralization processes (Helfenstein et al., 2018; Weihrach & Opp, 2018), with less clear trends in the specific extreme desert studied here. Likely, these fluctuations in organic P also reflect a certain spatial patchiness of rainfall and life in this hyper-arid region (Alcayaga et al., 2022; Knief et al., 2020; Merklinger et al., 2020). The intracellular cycling of P by inorganic pyrophosphatase is the most likely reaction to P turnover in the Atacama Desert, and the phosphate released from microbial cells can precipitate as secondary Ca-P minerals (Helfenstein et al., 2018; Shen et al., 2020). As a result, also the quantified contribution of Ca-bound P_o to total P_o increases with increasing aridity (Figure 5b). Consequently, the Ca-P pool derived from both parental material and biologically recycled P.

Here, we differentiated between geochemical and biological P sources by assessing the stable oxygen isotope values of HCl-extractable P_i ($\delta^{18}\text{O}_{\text{HCl-P}_i}$; Gross & Angert, 2015; Stout et al., 2014; Wang, Moradi, et al., 2021). At 2.3 km near the coast in the absence of plants, this isotopic value clearly differed from that of the parental material and with $17.8 \pm 0.9\%$, it even falls into the range of phosphate isotope signatures equilibrated solely with rainwater (16.7–22.8‰). By using rainfall water values, we obtain that the maximum percentage of biologically cycled P is over 100% (Table 1). This implies that there is another source of available water for soil biomass to recycle P across the sampling depth, which we attribute to the utilization of fog (Figure 6b).

The $\delta^{18}\text{O}_{\text{HCl-P}_i}$ values of other sites deviated from the $\delta^{18}\text{O}_{\text{HCl-P}_i}$ equilibrium ranges calculated based on either the fog or the rainfall $\delta^{18}\text{O}$ isotopic composition (Table 1, Figure 6b). Consequently, and unlike the near-coastal topsoil (see above) or in other ecosystems (Bauke et al., 2018; Gross et al., 2015; Hacker et al., 2019), inland moisture is insufficient to activate biological activity to a degree that soil P in the HCl-P was completely biologically cycled. The result supports the conclusion that the signature of $\delta^{18}\text{O}_{\text{HCl-P}_i}$ traces

past biological P cycling across centennial to millennial scales rather than being determined by short-term rainfall events in the hyper-arid region of the desert (Shen et al., 2020; Wang, Moradi, et al., 2021). The value of $\delta^{18}\text{O}_{\text{HCl-P}_i}$ correlated significantly and negatively with the concentration of P_i in the HCl-Hedley extracts (Ca-P; Figure 7a), following the non-linear increase of the portions of HCl- P_i with increasing distance to the coast. The concentrations of HCl- P_i reflected the apatite dissolution process. When less P becomes available through the weathering of primary minerals, there is also less P that can be taken up, biologically cycled, and finally re-precipitated by soil microorganisms (Blake et al., 2005; Jaisi et al., 2011; Tamburini et al., 2012). We thus conclude that limitations in the biological cycling of P in the Atacama Desert reflect limitations by physiochemical weathering, both being controlled by the limited amount of water supply (Frkova et al., 2022; Prietzel et al., 2018). However, in addition to these past studies cited, this study now shows that this water limitation was mainly caused by advective fog blocked from entering the inner part of the Atacama Desert.

4.2 | Non-linear changes of P dynamics with distance to coast

Many soil processes do not respond linearly to extrinsic variations of environmental factors (Bateman et al., 2019; Berdugo et al., 2020; Vitousek & Chadwick, 2013). We also observed non-linear rather than linear changes for all Hedley P_t and P_i concentrations, the portions of HCl-P in P_i pool and P_o pool, and for soil $\delta^{18}\text{O}_{\text{HCl-P}_i}$ values with increasing distance to the coast (Figures 4–6). Our data thus support earlier findings of the depletion of apatite P with increasing precipitation in the Atacama Desert (Brucker & Spohn, 2019). This lack of linearity likely reflects non-linear dependencies in water availability along the spatial gradients (Böhm et al., 2020, 2021; Knief et al., 2020). Furthermore, key water sources might have changed along the gradient, that is, from fog-dominated to solely fed by rare rainfall events.

In our study, fog occurrence frequency, as an index for the fog water availability, decreased non-linear along the transect (Figure 6a, Table S6). Various factors, such as topography, vegetation, wind patterns, and local climatic conditions, can influence the distribution and intensity of fog, resulting in a non-linear relationship between distance from the coast and fog occurrence frequency (Böhm et al., 2021; Cereceda et al., 2008b; Garcia et al., 2021). Using a standard fog collector (SFC), which is made of a fixed vertically erected mesh panel (Schemenauer & Cereceda, 1994), the fog water yield collected above 2m at a Paposito site 750 m a.s.l. (ca. 4.3 km from the coast) averages to 3.36 mm day^{-1} (Larrain et al., 2002; Figure S1). This corresponds to a potential availability of fog water of $3.36 \text{ mm day}^{-1} \times 365 \text{ days} = 1226 \text{ mm a}^{-1}$. Not all of this reaches the ground. Lehnert et al. (2018) found that a range of 8%–24% of the fog water collected by a cylindrical fog collector could be effectively utilized to nourish a biological soil crust in the Atacama Desert. The

annual deposition of fog water to the ground within the Paposito transect 4.3 km distance to coast can roughly be estimated to range between 98 and 294 mm. The potential water availability from fog thus exceeds that from MAP by more than one order of magnitude in coastal sites (Figure 6a, Table S1). Furthermore, the availability of fog water is consistent, with daily occurrences during the winter season, while precipitation may be absent for several consecutive years, only appear for one to three episodes of some minutes with rain in a particularly wet year, and also not infiltrating all into ground due to strong evaporation from crusted soil. Overall, the potential fog water availability thus shapes the change of aridity in the study area, making it reasonable that fog water explains the majority of P cycling near the coast.

The portions of HCl-P and its $\delta^{18}\text{O}_{\text{HCl-P}_i}$ value change most strongly at a transition to reaching a plateau, that is, in the fog-affected areas 2–10 km away from the coast but hardly beyond (Figures 4–6). The point where soil properties and processes change from nonlinear manner to constancy or small range of changes with increased environmental forcing is named “pedogenic thresholds”, which coincided here with the spatial limit of fog penetration into the desert (Bateman et al., 2019; Vitousek et al., 2016; Vitousek & Chadwick, 2013). Our data partly disagree with conclusions of Shen et al. (2020) who stated that sporadic gypsum hydration water were likely the key moisture sources for soil life in the Atacama Desert. Their assumption was based on full $\delta^{18}\text{O}$ isotope equilibrium of soil phosphates with ambient water. Our data, however, point to clear impacts from fog, particularly nearby the coast. Though MAP is almost constant from site 5.1 km to inland 22.9 km (Figure 6a), the values of $\delta^{18}\text{O}_{\text{HCl-P}_i}$ are significantly higher in the fog-nourished zone (5.1–10 km) compared to the inland area (≥ 10 km; Figure 6b, Table S3). Only $24 \pm 14\%$ of HCl- P_i in inland regions (≥ 10 km) can be explained by equilibration processes derived from isotope exchange with rainfall water only (Table 1). The significant correlation between $\delta^{18}\text{O}_{\text{HCl-P}_i}$ with fog occurrence frequency further supports the impact of fog on soil P nutrient cycling (Figure 7b). Therefore, we rank fog rather than crystalline water or hydration water as the most important, though not necessarily exclusive, source of water for microorganisms in western, near-coastal Atacama Desert.

The theoretical value of pedogenic thresholds is usually calculated based on a breakpoint model (Bateman et al., 2019; Vitousek et al., 2016; Vitousek & Chadwick, 2013). We calculated it as the point where the unit-distance increase was less than 0.1 of absolute value of the respective parameter. It means that the parameters were relatively constant beyond the calculated distances (Table 2, Equation 5). It occurred 11.7 km away from the coast (by $\delta^{18}\text{O}_{\text{HCl-P}_i}$), thus exceeding the upper limit of fog around 7.6 km. Hence, also other factors can be interpreted to additionally affect the availability of P_i in the HCl-P pool, such as release from organic P forms, immobilization of P_i by other minerals like oxides, anthropogenic depositions and high salinity as discussed previously for the outliner at 17.3 km distance to coast, or the patchy distribution of occasional rain (Table 2, Figures 3 and 4); yet, given the close fit, fog still remains the dominating factor.

4.3 | Local-scale disturbance on P cycling by plant growth

Brucker and Spohn (2019) forwarded that plant cover was the driving factor for “pedogenic thresholds”, because plants can enhance apatite dissolution by uptake of phosphate, as well as by increasing the solubility of P with releasing siderophores and other chelators or acids (Hinsinger, 2001). Similar to HCl-P and $\delta^{18}\text{O}_{\text{HCl-P}_i}$ isotopic composition, also plant cover changed non-linearly to a minimum with increasing distance to the coast (Figure S2). However, mean $\delta^{18}\text{O}_{\text{HCl-P}_i}$ values and HCl-P pool did not change significantly (Table S3). Instead, samples collected near the plant showed lower concentration of Resin-P but enhanced portions of P in the Fe/Al-P_o and residual P pool (Table S3). Hence, plants affected P dynamics, but apparently not through apatite weathering. Two reasons may account for this. On the one hand, there is an increased water use by plants: when plants utilize P they also consume water, which is then not available for apatite dissolution. Likely, the potential acceleration of P release from minerals by specific exudation was compensated by a deceleration of P release under dryer conditions. On the other hand, the patchy distribution of rainfall and blooming vegetation might not be representative for the rhizosphere-affected soil at the time of sampling, when plants grew at other places with different rainfall patterns decades and centuries ago. The latter argument supports the potential explanation for the lack of a relationship between plant growth and SAR (Figure 3, Tables S2 and S4). The idea reinforces Wang, Moradi, et al. (2021) who state that the biological P cycling hardly reflects a seasonal impact on soil chemistry but an integral of decades to millennia. It is in accordance with the findings of Mörchen et al. (2021), who identified plant-biomarkers in Atacama soils at places without visible plant growth during sampling. Additionally, there can be site-specific individual variations of halophytic plant growth and its respective strategies to cope with osmotic stress (Brucker & Spohn, 2019; Mörchen et al., 2021), together with some site-specific preferences of plant growth to moisture niches which feature lower accumulation of salts.

5 | CONCLUSIONS

Our data support our first hypothesis that fog predominantly sustains biological soil P cycling in the Atacama Desert. Beyond the 10km range from the coastline, additional water supply from fog becomes scarce, and rare occasional rainfall events enable the release of apatite-bound phosphate and modify its oxygen isotope composition. However, observed changes in inland areas were significantly smaller compared to those detected in coastal regions. The second hypothesis was also confirmed: the range of the coastal fog penetration into the desert was a key threshold for biological soil P cycling and thus likely also for climate-controlled expansion of soil life in the Atacama Desert. However, the third hypothesis has to be rejected: the current presence of plants on

biological P cycling was not found to affect the soil phosphate isotope signatures sufficiently to allow detection by stable-isotope oxygen tracing in the HCl-P pool, either because the current distribution of plants is not representative of that in the past or because the additional consumption of soil water interfered with the biological cycling of P.

AUTHOR CONTRIBUTIONS

Xiaolei Sun: Conceptualization; data curation; formal analysis; investigation; validation; visualization; writing – original draft; writing – review and editing. **Wulf Amelung:** Conceptualization; data curation; funding acquisition; methodology; project administration; supervision; writing – original draft; writing – review and editing. **Erwin Klumpp:** Conceptualization; funding acquisition; investigation; project administration; resources; supervision; writing – review and editing. **Janek Walk:** Investigation; visualization; writing – review and editing. **Ramona Mörchen:** Resources; writing – review and editing. **Christoph Böhm:** Visualization; writing – original draft; writing – review and editing. **Ghazal Moradi:** Investigation. **Simon Matthias May:** Visualization; writing – review and editing. **Federica Tamburini:** Investigation; methodology; writing – review and editing. **Ye Wang:** Investigation. **Roland Bol:** Conceptualization; funding acquisition; investigation; project administration; resources; supervision; writing – review and editing.

ACKNOWLEDGEMENTS

This work was done as part of the Collaborative Research Center 1211: “Earth–Evolution at the Dry Limit,” funded by the Deutsche Forschungsgemeinschaft (DFG, German Research Foundation)–Projektnummer 268236062-SFB 1211. Xiaoli Sun thanks the China Scholarship Council (CSC:201904910544) for supporting her study at RWTH Aachen University and Forschungszentrum Jülich. The authors would like to thank Dr. Sara Bauke (University of Bonn) for support with the preparation of silver phosphate for measuring $\delta^{18}\text{O}_{\text{HCl-P}_i}$. Open Access funding enabled and organized by Projekt DEAL.

CONFLICT OF INTEREST STATEMENT

The authors declare that they have no competing interests.

DATA AVAILABILITY STATEMENT

The data that support the findings of this study are available in Data Dryad at: <https://doi.org/10.5061/dryad.ncjsxkt20>.

ORCID

Xiaolei Sun  <https://orcid.org/0000-0002-5117-812X>

Wulf Amelung  <https://orcid.org/0000-0002-4920-4667>

Erwin Klumpp  <https://orcid.org/0000-0002-4810-9414>

Janek Walk  <https://orcid.org/0000-0002-3283-7214>

Ramona Mörchen  <https://orcid.org/0000-0002-3955-6490>

Christoph Böhm  <https://orcid.org/0000-0001-8712-3318>

Simon Matthias May  <https://orcid.org/0000-0001-6762-7500>

Federica Tamburini  <https://orcid.org/0000-0001-6871-1915>

Roland Bol  <https://orcid.org/0000-0003-3015-7706>

REFERENCES

- Alcayaga, H., Soto-Alvarez, M., Laronne, J. B., Caamaño, D., Mao, L., & Urrutia, R. (2022). Runoff volume and sediment yield from an endorheic watershed generated by rare rainfall events in the Atacama Desert. *Geomorphology*, *400*(1), 108107.
- Allmendinger, R. W., & González, G. (2010). Invited review paper: Neogene to Quaternary tectonics of the coastal Cordillera, Northern Chile. *Tectonophysics*, *495*(1–2), 93–110.
- Álvarez, J., Jorquera, R., Miralles, C., Padel, M., & Martínez, P. (2016). Cartas Punta Posallaves y Sierra Vicuña Mackenna, Región de Antofagasta, Serie Geología Básica 183–184, 147 pp., 1 mapa escala 1:100.000. Servicio Nacional de Geología y Minerías, Santiago.
- Amelung, W., Antar, P., Kleeberg, I., Oelmann, Y., Luecke, A., Alt, F., Lewandowski, H., Paetzold, S., & Barej, J. A. M. (2015). The $\delta^{18}\text{O}$ signatures of HCl-extractable soil phosphate: Methodological challenges and evidence of the cycling of biological P in arable soil. *European Journal of Soil Science*, *66*, 965–972. <https://doi.org/10.1111/ejss.12288>
- Angert, A., Weiner, T., Mazeh, S., & Sternberg, M. (2012). Soil phosphate stable oxygen isotopes across rainfall and bedrock gradients. *Environmental Science & Technology*, *46*, 2156–2162. <https://doi.org/10.1021/es203551s>
- Aravena, R., Suzuki, O., Pena, H., Pollastri, A., Fuenzalida, H., & Grilli, A. (1999). Isotopic composition and origin of the precipitation in Northern Chile. *Applied Geochemistry*, *14*, 411–422.
- Aravena, R., Suzuki, O., & Pollastri, A. (1989). Coastal fog and its relation to groundwater in the IV region of northern Chile. *Chemical Geology (Isotope Geoscience Section)*, *79*, 83–91.
- Arenas-Díaz, F., Fuentes, B., Reyers, M., Fiedler, S., Böhm, C., Campos, E., Shao, Y., & Bol, R. (2022). Dust and aerosols in the Atacama Desert. *Earth-Science Reviews*, *226*, 103925.
- Arens, F. L., Airo, A., Feige, J., Sager, C., Wiechert, U., & Schulze-Makuch, D. (2021). Geochemical proxies for water-soil interactions in the hyperarid Atacama Desert, Chile. *Catena*, *206*, 105531.
- Arndt, H., Ritter, B., Rybarski, A., Schiwitza, S., Dunai, T., & Nitsche, F. (2020). Mirroring the effect of geological evolution: Protist divergence in the Atacama Desert. *Global and Planetary Change*, *190*, 103193.
- Azúa-Bustos, A., González-Silva, C., Mancilla, R. A., Salas, L., Gómez-Silva, B., McKay, C. P., & Vicuña, R. (2011). Hypolithic cyanobacteria supported mainly by fog in the coastal range of the Atacama Desert. *Environmental Microbiology*, *61*(3), 568–581.
- Bateman, J. B., Chadwick, O. A., & Vitousek, P. M. (2019). Quantitative analysis of pedogenic thresholds and domains in volcanic soils. *Ecosystems*, *22*(7), 1633–1649.
- Bauke, S. L., von Sperber, C., Tamburini, F., Gocke, M. I., Honermeier, B., Schweitzer, K., Baumecker, M., Don, A., Sandhage-Hofmann, A., & Amelung, W. (2018). Subsoil phosphorus is affected by fertilization regime in long-term agricultural experimental trials. *European Journal of Soil Science*, *69*(1), 103–112.
- Bauke, S. L., Wang, Y., Saia, S. M., Popp, C., Tamburini, F., Paetzold, S., Amelung, W., & Sperber, C. V. (2022). Phosphate oxygen isotope ratios in vegetated riparian buffer strip soils. *Vadose Zone Journal*, *21*(3), e20193.
- Berdugo, M., Delgado-Baquerizo, M., Soliveres, S., Hernández-Clemente, R., Zhao, Y., Gaitán, J. J., Gross, N., Saiz, H., Maire, V., Lehmann, A., Rillig, M. C., Solé, R. V., & Maestre, F. T. (2020). Global ecosystem thresholds driven by aridity. *Science*, *367*, 787–790.
- Bernhard, N., Moskwa, L., Schmidt, K., Oeser, R. A., Aburto, F., Bader, M. Y., Baumann, K., Blanckenburg, F. V., Boy, J., Brink, L. V. D., Brucker, E., Büdel, B., Canessa, R., Dippold, M. A., Ehlers, T. A., Fuentes, J. P., Godoy, R., Jung, P., Karsten, U., ... Kühn, P. (2018). Pedogenic and microbial interrelations to regional climate and local topography: New insights from a climate gradient (arid to humid) along the Coastal Cordillera of Chile. *Catena*, *170*, 335–355.
- Bischoff, N., Mikutta, R., Shibistova, O., Dohrmann, R., Herdtle, D., Gerhard, L., Fritzsche, F., Puzanov, A., Silanteva, M., Grebennikova, A., & Guggenberger, G. (2018). Organic matter dynamics along a salinity gradient in Siberian steppe soils. *Biogeosciences*, *15*, 13–29.
- Blake, R. E., Chang, S. J., & Lepland, A. (2010). Phosphate oxygen isotopic evidence for a temperate and biologically active Archaean Ocean. *Nature*, *464*, 1029–1032.
- Blake, R. E., O'Neil, J. R., & Surkov, A. V. (2005). Biogeochemical cycling of phosphorus: Insights from oxygen isotope effects of phosphoenzymes. *American Journal of Science*, *305*, 596–620.
- Böhm, C., Reyers, M., Schween, J. H., & Crewell, S. (2020). Water vapor variability in the Atacama Desert during the 20th century. *Global and Planetary Change*, *190*, 103192.
- Böhm, C., Schween, J. H., Reyers, M., Maier, B., Löhnert, U., & Crewell, S. (2021). Toward a climatology of fog frequency in the Atacama Desert via multispectral satellite data and machine learning techniques. *Journal of Applied Meteorology and Climatology*, *60*(8), 1149–1169.
- Boschetti, T., Cifuentes, J., Lacumin, P., & Selmo, E. (2019). Local meteoric water line of northern Chile (18°S–30°S): An application of error-in variables regression to the oxygen and hydrogen stable isotope ratio of precipitation. *Water*, *11*, 791.
- Boy, D., Moeller, R., Sauheitl, L., Schaarschmidt, F., Rapp, S., Brink, L. V. D., Gschwendtner, S., Godoy Borquez, R., Matus, F. J., Horn, M. A., Guggenberger, G., & Boy, J. (2022). Gradient studies reveal the true driver of extreme life in the Atacama Desert. *JCR Biogeosciences*, *127*(3), e2021JG006714. <https://doi.org/10.1029/2021JG006714>
- Brucker, E., & Spohn, M. (2019). Formation of soil phosphorus fractions along a climate and vegetation gradient in the coastal cordillera of Chile. *Catena*, *180*, 203–211.
- Bünemann, E. K. (2015). Assessment of gross and net mineralization rates of soil organic phosphorus—A review. *Soil Biology and Biochemistry*, *89*, 82–98.
- Cáceres, L., Gómez-Silva, B., Garró, X., Rodríguez, V., Monardes, V., & McKay, C. P. (2007). Relative humidity patterns and fog water precipitation in the Atacama Desert and biological implications. *Journal of Geophysical Research*, *112*, G04S14. <https://doi.org/10.1029/2006JG000344>
- Cappa, C. D., Hendricks, M. B., DePaolo, D. J., & Cohen, R. C. (2003). Isotopic fractionation of water during evaporation. *Journal of Geophysical Research-Atmospheres*, *108*(D16), 4525. <https://doi.org/10.1029/2003JD003597>
- Cereceda, P., Larrain, H., Osses, P., Fariás, M., & Egaña, I. (2008a). The climate of the coast and fog zone in the Tarapacá region, Atacama Desert, Chile. *Atmospheric Research*, *87*(3), 301–311.
- Cereceda, P., Larrain, H., Osses, P., Fariás, M., & Egaña, I. (2008b). The spatial and temporal variability of fog and its relation to fog oases in the Atacama Desert, Chile. *Atmospheric Research*, *87*(3–4), 312–323.
- Cereceda, P., Osses, P., Larrain, H., Fariás, M., Lagos, M., Pinto, R., & Schemenauer, R. (2002). Advective, orographic and radiation fog in the Tarapacá region, Chile. *Atmospheric Research*, *64*, 261–271.
- Chand, D., Hegg, D. A., Wood, R., Shaw, G. E., Wallace, D., & Covert, D. S. (2010). Source attribution of climatically important aerosol properties measured at Papos (Chile) during VOCALS. *Atmospheric Chemistry and Physics*, *10*(22), 10789–10801.
- Chang, S. J., & Blake, R. E. (2015). Precise calibration of equilibrium oxygen isotope fractionations between dissolved phosphate and water from 3 to 37°C. *Geochimica et Cosmochimica Acta*, *150*, 314–329.

- Chávez, R. O., Moreira-Muñoz, A., Galleguillos, M., Olea, M., Aguayo, J., Latín, A., Aguilera-Betti, I., Muñoz, A. A., & Manríquez, H. (2019). GIMMS NVDI time series reveal the extent, duration and intensity of "blooming desert" events in the hyper-arid Atacama Desert, Northern Chile. *International Journal of Applied Earth Observation and Geoinformation*, 76, 193–203.
- Chen, C. R., Hou, E. Q., Condrón, L. M., Bacon, G., Esfandbod, M., Olley, J., & Turner, B. L. (2015). Soil phosphorus fractionation and nutrient dynamics along the Cooloola coastal dune chronosequence, southern Queensland, Australia. *Geoderma*, 257–258, 4–13.
- Dawson, T. E., & Goldsmith, G. R. (2018). The value of wet leaves. *New Phytologist*, 219, 1156–1169. <https://doi.org/10.1111/nph.15307>
- Dunai, T. J., González López, G. A., & Juez-Larré, J. (2005). Oligocene–Miocene age of aridity in the Atacama Desert revealed by exposure dating of erosion-sensitive landforms. *Geology*, 33, 321–324. <https://doi.org/10.1130/G21184.1>
- Dunai, T. J., Melles, M., Quandt, D., Knief, C., & Amelung, W. (2020). Whitepaper: Earth–evolution at the dry limit. *Global and Planetary Change*, 193, 103275.
- Escribano, J., Martínez, P., Domagala, J., Padel, M., Espinoza, M., Jorquera, R., Contreras, J. P., De La Cruz, R., & Calderón, M. (2013). Cartas Bahía Isla Blanca y Taltal, Región de Antofagasta, Serie Geología Básica 164–165, 75 pp., 1 mapa escala 1:100.000. Servicio Nacional de Geología y Minería, Santiago. <https://tiendadigital.sernageomin.cl/en/-basic-geology/3180-cartas-bahia-isla-blanca-y-taltal-regio-n-de-antofagasta.html>
- Eshel, G., Arous, V., Undurraga, S., Soto, D. C., Moraga, C., Montecinos, A., Moyano, T., Maldonado, J., Díaz, F. P., Varala, K., Nelson, C. W., Contreras-López, O., Pal-Gabor, H., Kraiser, T., Carrasco-Puga, G., Nilo-Poyanco, R., Zegar, C. M., Orellana, A., Montecino, M., ... Gutiérrez, R. (2021). Plant ecological genomics at the limits of life in the Atacama Desert. *Proceedings of the National Academy of Sciences of the United States of America*, 118(46), e2101177118. <https://doi.org/10.1073/pnas.2101177118>
- Evenstar, L., Mather, A. E., Hartley, A. J., Stuart, F. M., Sparks, R. S. J., & Cooper, F. J. (2017). Geomorphology on geologic timescales: Evolution of the late Cenozoic Pacific paleosurface in Northern Chile and Southern Peru. *Earth-Science Reviews*, 171, 1–27.
- Ewing, S. A., Sutter, B., Owen, J., Nishiizumi, K., Sharp, W., Cliff, S. S., Perry, K., Diettrich, W., McKay, C. P., & Amundson, R. (2006). A threshold in soil formation at Earth's arid-hyperarid transition. *Geochimica et Cosmochimica Acta*, 70, 5293–5322.
- Farhangi-Abri, S., & Ghassemi-Golezani, K. (2021). Changes in soil properties and salt tolerance of safflower in response to biochar-based metal oxide nanocomposites of magnesium and manganese. *Ecotoxicology and Environmental Safety*, 211, 111904.
- Farr, T. G., Rosen, P. A., Caro, E., Crippen, R., Duren, R., Hensley, S., Kobrick, M., Paller, M., Rodriguez, E., Roth, L., Seal, D., Shaffer, S., Shimada, J., Umland, J., Werner, M., Oskin, M., Burbank, D., & Alsdorf, D. (2007). The shuttle radar topography mission. *Reviews of Geophysics*, 45(2), RG2004. <https://doi.org/10.1029/2005RG000183>
- Feng, J., Turner, B. L., Lü, X., Chen, Z., Wei, K., Tian, J., Wang, C., Luo, W., & Chen, L. (2016). Phosphorus transformations along a large-scale climosequence in arid and semiarid grasslands of northern China. *Global Biogeochemical Cycles*, 30, 1264–1275. <https://doi.org/10.1002/2015GB005331>
- Fessehay, M., Abdul-Wahab, S. A., Savage, M. J., Kohler, T., Gherezghier, T., & Hurni, H. (2014). Fog-water collection for community use. *Renewable and Sustainable Energy Reviews*, 29, 52–62.
- Fick, S. E., & Hijmans, R. J. (2017). WorldClim 2: New 1-km spatial resolution climate surfaces for global land areas. *International Journal of Climatology*, 37, 4302–4315. <https://doi.org/10.1002/joc.5086>
- Frkova, Z., Pistocchi, C., Vystavna, Y., Capkova, K., Dolezal, J., & Tamburini, F. (2022). Phosphorus dynamics during early soil development in a cold desert: Insights from oxygen isotope in phosphate. *The Soil*, 8, 1–15.
- Fuentes, B., Choque, A., Gómez, F., Alarcón, J., Castro-Nallar, E., Arenas, F., Contreras, D., Mörchen, R., Amelung, W., Knief, C., Moradi, G., Klumpp, E., Saavedra, C. P., Prietzel, J., Klysubun, W., Remonsellez, F., & Bol, R. (2022). Influence of physical-chemical soil parameters on microbiota composition and diversity in a deep hyperarid core of the Atacama Desert. *Frontiers in Microbiology*, 12, 794743. <https://doi.org/10.3389/fmicb.2021.794743/full>
- Fuentes, B., Gómez, F., Valdez, C., Videla, A., Castro-Severyn, J., Barahona, S., Bol, R., Riquelme, R., Quispe, J., & Remonsellez, F. (2022). Effects of altitude on soil properties in coastal fog ecosystems in Morro Moreno National Park, Antofagasta, Chile. *European Journal of Soil Science*, 73, e13217. <https://doi.org/10.1111/ejss.13217>
- Gallardo, A., Fernández-Palacios, J. M., Bermúdez, A., de Nascimento, L., Durán, J., García-Velázquez, L., Méndez, J., & Rodríguez, A. (2020). The pedogenic Walker and Syers model under high atmospheric P deposition rates. *Biogeochemistry*, 148, 237–253. <https://doi.org/10.1007/s10533-020-00657-8>
- García, J. L., Lobos-Roco, F., Schween, J. H., Río, C. D., Osses, P., Vives, R., Pezoa, M., Siegmund, A., Latorre, C., Alfaro, F., Koch, M. A., & Loehnert, U. (2021). Climate and coastal low-cloud dynamic in the hyperarid Atacama fog desert and the geographic distribution of *Tillandsia landbeckii* (Bromeliaceae) dune ecosystems. *Plant Systematics and Evolution*, 307, 57. <https://doi.org/10.1007/s00606-021-01775-y>
- Garreaud, R., Barichivich, J., Christie, D. A., & Maldonado, A. (2008). Interannual variability of the coastal fog at Fray Jorge relict forests in semiarid Chile. *Journal of Geophysical Research*, 113, G04011. <https://doi.org/10.1029/2008JG000709>
- González, G., Cembrano, J., Carrizo, D., Macci, A., & Schneider, H. (2003). The link between forearc tectonics and Pliocene–Quaternary deformation of the Coastal Cordillera, Northern Chile. *Journal of South American Earth Sciences*, 16, 321–342. [https://doi.org/10.1016/S0895-9811\(03\)00100-7](https://doi.org/10.1016/S0895-9811(03)00100-7)
- González-Pinilla, F. J., Latorre, C., Rojas, M., Houston, J., Rocuant, M. I., Maldonado, A., Santoro, C. M., Quade, J., & Betancourt, J. L. (2021). High- and low-latitude forcings drive Atacama Desert rainfall variations over the past 16,000 years. *Science Advances*, 7, eabg1333. <https://doi.org/10.1126/sciadv.abg1333>
- Gross, A., & Angert, A. (2015). What processes control the oxygen isotopes of soil bio-available phosphate? *Geochimica et Cosmochimica Acta*, 159, 100–111.
- Gross, A., Turner, B. L., Wright, S. J., Tanner, E. V. J., Reichstein, M., Weiner, T., & Angert, A. (2015). Oxygen isotope ratios of plant available phosphate in lowland tropical forest soils. *Soil Biology and Biochemistry*, 88, 354–361.
- Hacker, N., Wilcke, W., & Oelmann, Y. (2019). The oxygen isotope composition of bioavailable phosphate in soils reflects the oxygen isotope composition in soil water driven by plant diversity effects on evaporation. *Geochimica et Cosmochimica Acta*, 248, 387–399.
- Hartley, A. J., Chong, G., Houston, J., & Mather, A. E. (2005). 150 million years of climatic stability: Evidence from the Atacama Desert, Northern Chile. *Journal of the Geological Society*, 162, 421–424. <https://doi.org/10.1144/0016-764904-071>
- Hedley, M. J., Stewart, J. W. B., & Chauhan, B. S. (1982). Changes in inorganic and organic phosphorus fractions induced by cultivation practices and by laboratory incubations. *Soil Science Society of America Journal*, 46, 970–976. <https://doi.org/10.2136/sssaj1982.03615995004600050017x>
- Helfenstein, J., Tamburini, F., von Sperber, C., Massey, M. S., Pistocchi, C., Chadwick, O. A., Vitousek, P. M., Kretschmar, R., & Frossard, E. (2018). Combining spectroscopic and isotopic techniques gives a dynamic view of phosphorus cycling in soil. *Nature Communications*, 9, 3226.

- Hinsinger, P. (2001). Bioavailability of soil inorganic P in the rhizosphere as affected by root-induced chemical changes: A review. *Plant and Soil*, 237, 173–195.
- Hoffmeister, D. (2018). *Meteorological and soil measurements of the permanent weather stations in the Atacama desert, Chile*. CRC1211 Database (CRC1211DB). <https://www.crc1211db.uni-koeln.de/DOI/doi.php?doiID=1>
- Houston, J. (2006). Variability of precipitation in the Atacama Desert: Its causes and hydrological impact. *International Journal of Climatology*, 26, 2181–2198. <https://doi.org/10.1002/joc.1359>
- Izquierdo, J. E., Houlton, B. Z., & van Huysen, T. L. (2013). Evidence for progressive phosphorus limitation over long-term ecosystem development: Examination of a biogeochemical paradigm. *Plant and Soil*, 367, 135–147. <https://doi.org/10.1007/s11104-013-1683-3>
- Jaisi, D. P., & Blake, R. E. (2010). Tracing sources and cycling of phosphorus in Peru Margin sediments using oxygen isotopes in authigenic and detrital phosphates. *Geochimica et Cosmochimica Acta*, 74(11), 3199–3212.
- Jaisi, D. P., Kukkadapu, R. K., Stout, L. M., Varga, T., & Blake, R. E. (2011). Biotic and abiotic pathways of phosphorus cycling in minerals and sediments: Insights from oxygen isotope ratios in phosphate. *Environmental Science & Technology*, 45(15), 6254–6261. <https://doi.org/10.1021/es200456e>
- Jordan, T., Riquelme, R., González, G., Herrera, C., Godfrey, L., Colucci, S., Gironás León, J., Gamboa, C., Urrutia, J., Tapia, L., Centella, K., & Ramos, H. (2015). Hydrological and geomorphological consequences of the extreme precipitation event of 24–26 March 2015, Chile. XIV Congreso Geológico Chileno (La Serena), 777–780. https://catalogobiblioteca.sernageomin.cl/Archivos/14905_v2_pp_777_780.pdf
- Jordan, T. E., Herrera, C., Godfrey, L. V., Colucci, S. J., Gamboa, C., Urrutia, J., Gonzalez, G., & Paul, J. F. (2019). Isotopic characteristics and paleoclimate implications of the extreme precipitation event of March 2015 in Northern Chile. *Andean Geology*, 46, 1–31.
- Knief, C., Bol, R., Amelung, W., Kusch, S., Frindte, K., Eckmeier, E., Jaeschke, A., Dunai, T., Fuentes, B., Mörchen, R., Schütte, T., Lücke, A., Klumpp, E., Kaise, K., & Rethermeyer, J. (2020). Tracing elevational changes in microbial life and organic carbon sources in soils of the Atacama Desert. *Global and Planetary Change*, 184, 103078.
- Larrain, H., Velásquez, F., Cereceda, P., Espejo, R., Pinto, R., Osses, P., & Schemenauer, R. S. (2002). Fog measurements at the site “Falda Verde” north of Chañaral compared with other fog stations of Chile. *Atmospheric Research*, 64, 273–284.
- Lehnert, L. W., Thies, B., Trachte, K., Achilles, S., Osses, P., Baumann, K., Schmidt, J., Samolov, E., Jung, P., Leinweber, P., Karsten, U., Büdel, B., & Bendix, J. (2018). A case study on fog/low stratus occurrence at Las Lomitas, Atacama Desert (Chile) as a water source for biological soil crusts. *Aerosol and Air Quality Research*, 18(1), 254–269. <https://doi.org/10.4209/aaqr.2017.01.0021>
- Li, C., Fu, B., Wang, S., Stringer, L. C., Wang, Y., Li, Z., Liu, Y., & Zhou, W. (2021). Drivers and impacts of changes in China's drylands. *Nature Reviews Earth & Environment*, 2, 858–873.
- Li, J., Wang, F., Michalski, G., & Wilkins, B. (2019). Atmospheric deposition across the Atacama Desert, Chile: Compositions, source distributions, and interannual comparisons. *Chemical Geology*, 525, 435–446.
- Lickley, M., & Solomon, S. (2018). Drivers, timing and some impact of global aridity change. *Environmental Research Letters*, 13, 104010. <https://doi.org/10.1088/1748-9326/aae013>
- Liu, L., Gudmundsson, L., Hauser, M., Qi, B., Li, S., & Seneviratne, S. I. (2020). Soil moisture dominates dryness stress on ecosystem production globally. *Nature Communications*, 11, 4892.
- Margalef, O., Sardans, J., Maspons, J., Molowny-Horas, R., Fernández-Martínez, M., Janssens, I. A., Richter, A., Ciais, P., Obersteiner, M., & Peñuelas, J. (2021). The effect of global change on soil phosphatase activity. *Global Change Biology*, 27(22), 5989–6003.
- Merklinger, F. F., Zheng, Y., Luerbert, F., Harpke, D., Böhnert, T., Stoll, A., Koch, M. A., Blattner, F. R., Wiehe, T., & Quandt, D. (2020). Population genomics of *Tillandsia landbeckii* reveals unbalanced genetic diversity and founder effects in the Atacama Desert. *Global and Planetary Change*, 184, 103076.
- Moat, J., Orellana-García, A., Tovar, C., Arakaki, M., Arana, C., Cano, A., Faundez, L., Cardner, M., Hechenleitner, P., Hepp, J., Lewis, G., Mamani, J., Miyasiro, M., & Whaley, O. Q. (2021). Seeing through the clouds – Mapping desert fog oasis ecosystems using 20 years of MODIS imagery over Peru and Chile. *International Journal of Applied Earth Observation and Geoinformation*, 103, 102468.
- MODIS Characterization Support Team. (2017a). *MOD021KM-Level 1B Calibrated Radiances-1 km*. NASA MODIS Adaptive Processing System, Goddard Space Flight Center. <https://doi.org/10.5067/MODIS/MOD021KM.061>
- MODIS Characterization Support Team. (2017b). *MYD021KM-Level 1B Calibrated Radiances-1 km*. NASA MODIS Adaptive Processing System, Goddard Space Flight Center <https://doi.org/10.5067/MODIS/MYD021KM.061>
- Moradi, G. (2023). Soil phosphorus in the extremely arid Atacama Desert. Dissertation/PhD Thesis, RWTH Aachen University, Aachen, Germany. <https://publications.rwth-aachen.de/record/957950>
- Moradi, G., Bol, R., Trbojevic, L., Missong, A., Mörchen, R., Fuentes, B., May, S. M., Lehdorff, E., & Klumpp, E. (2020). Contrasting depth distribution of colloid-associated phosphorus in the active and abandoned sections of an alluvial fan in a hyper-arid region of the Atacama Desert. *Global and Planetary Change*, 185, 103090.
- Mörchen, R., Amelung, W., Giese, C., Böhnert, T., Ruhm, J., & Lehdorff, E. (2021). Fingerprint of plant life in the Atacama Desert—Insights from n-alkane analyses. *Organic Geochemistry*, 151, 104145.
- Mörchen, R., Lehdorff, E., Diaz, F. A., Moradi, G., Bol, R., Fuentes, B., Klumpp, E., & Amelung, W. (2019). Carbon accrual in the Atacama Desert. *Global and Planetary Change*, 181, 102993.
- Oliveros, V., González, J., Espinoza Vargas, M., Vásquez, P., Rossel, P., Creixell, C., Sepúlveda, F., & Bastias, F. (2018). The early stages of the magmatic arc in the southern Central Andes. In A. Folguera, E. Contreras-Reyes, N. Heredia, A. Encinas, S. B. Iannelli, V. Oliveros, F. M. Dávila, G. Collo, L. Giambiagi, A. Maksymowicz, M. P. Iglesia Llanos, M. Turienzo, M. Naipauer, D. Orts, V. D. Litvak, O. Alvarez, & C. Arriagada (Eds.), *The evolution of the Chilean-Argentinean Andes* (pp. 165–190). Springer International Publishing. https://doi.org/10.1007/978-3-319-67774-3_7
- Ortega, C., Vargas, G., Rojas, M., Rutllant, J. A., Muñoz, P., Lange, C. B., Pantoja, S., Dezileau, L., & Ortlieb, L. (2019). Extreme ENSO-driven torrential rainfalls at the southern edge of the Atacama Desert during the Late Holocene and their projection into the 21st century. *Global and Planetary Change*, 175, 226–237.
- Palacio, S., Azorin, J., Montserrat-Martí, G., & Ferrio, J. P. (2014). The crystallization water of gypsum rocks is a relevant water source for plants. *Nature Communications*, 5, 4660.
- Pfeiffer, M., Morgan, A., Heimsath, A., Jordan, T., Howard, A., & Amundson, R. (2021). Century scale rainfall in the absolute Atacama Desert: Landscape response and implications for past and future rainfall. *Quaternary Science Reviews*, 254, 106797.
- Prietzl, J., Prater, I., Colocho Hurtarte, L. C., Hrbáček, F., Klysubun, W., & Mueller, C. W. (2018). Site conditions and vegetation determine phosphorus and sulfur speciation in soils of Antarctica. *Geochimica et Cosmochimica Acta*, 246, 339–362.
- Quade, J., Rech, J. A., Latorre, C., Betancourt, J. L., Gleeson, E., & Kalin, M. T. (2007). Soils at the hyperarid margin: The isotopic composition of soil carbonate from the Atacama Desert, Northern Chile. *Geochimica et Cosmochimica Acta*, 71, 3772–3795.
- Reed, S. C., Yang, X., & Thorntons, P. E. (2015). Incorporating phosphorus cycling into global modelling efforts: A worthwhile, tractable endeavor. *New Phytologist*, 208, 324–329.

- Roberts, K., Defforey, D., Turner, B. L., Condrón, L. M., Peek, S., Silva, S., Kendall, C., & Paytan, A. (2015). Oxygen isotopes of phosphate and soil phosphorus cycling across a 6500 year chronosequence under lowland temperate rainforest. *Geoderma*, 257–258, 14–21.
- Rothfuss, Y., Merz, S., Vanderborght, J., Hermes, N., Weuthen, A., Pohlmeier, A., Vereecken, H., & Brüggemann, N. (2015). Long-term and high-frequency non-destructive monitoring of water stable isotope profiles in an evaporating soil column. *Hydrology and Earth Systems Sciences*, 19, 4067–4080.
- Sáez, A., Cabrera, L., Garcés, M., van den Bogaard, P., Jensen, A., & Gimeno, D. (2012). The stratigraphic record of changing hyperaridity in the Atacama Desert over the last 10 Ma. *Earth and Planetary Science Letters*, 355–356, 32–38.
- Schemenauer, R. S., & Cereceda, P. (1994). A proposed standard fog collector for use in high-elevation regions. *Journal of Applied Meteorology and Climatology*, 33(11), 1313–1322.
- Scheuber, E., & González, G. (1999). Tectonics of the Jurassic–Early Cretaceous magmatic arc of the north Chilean Coastal Cordillera (22°–26°S): A story of crustal deformation along a convergent plate boundary. *Tectonics*, 18, 895–910. <https://doi.org/10.1029/1999TC900024>
- Schulz, N., Boisier, J. P., & Aceituno, P. (2012). Climate change along the arid coast of northern Chile. *International Journal of Climatology*, 32(12), 1803–1814.
- Schulze-Makuch, D., Wagner, D., Kounaves, S. P., Mangelsdorf, K., Devine, K. G., de Vera, J. P., Schmitt-Kopplin, P., Grossart, H. P., Parro, V., Kaupenjohann, M., Galy, A., Schneider, B., Airo, A., Frösler, J., Davila, A. F., Arens, F. L., Cáceres, L., Cornejo, F. S., Carrizo, D., ... Zamorano, P. (2018). Transitory microbial habitat in the hyperarid Atacama Desert. *Proceedings of the National Academy of Sciences of the USA*, 115(11), 2670–2675.
- Schween, J. H., Hoffmeister, D., & Löhnert, U. (2020). Filling the observational gap in the Atacama Desert with a new network of climate stations. *Global and Planetary Change*, 184, 103034.
- Selmants, P. C., & Hart, S. C. (2010). Phosphorus and soil development: Does the Walker and Syers model apply to semiarid ecosystems? *Ecology*, 91, 474–484.
- Shen, J., Smith, A. C., Claire, M. W., & Zerkle, A. L. (2020). Unravelling biogeochemical phosphorus dynamics in hyperarid Mars-analogue soils using stable oxygen isotopes in phosphate. *Geobiology*, 18, 760–779.
- Shen, J., Wyness, A. J., Claire, M. W., & Zerkle, A. L. (2021). Spatial variability of microbial communities and salt distributions across a latitudinal aridity gradient in the Atacama Desert. *Microbial Ecology*, 82, 442–458.
- Smith, A. C., Pfahler, V., Tamburini, F., Blackwell, M. S. A., & Granger, S. J. (2021). A review of phosphate oxygen isotope values in global bedrocks: Characterising a critical endmember to the soil phosphorus system. *Journal of Plant Nutrition and Soil Science*, 184, 25–34.
- Stout, L. M., Joshi, S. R., Kana, T. M., & Jaisi, D. P. (2014). Microbial activities and phosphorus cycling: An application of oxygen isotope ratios in phosphate. *Geochimica et Cosmochimica Acta*, 138, 101–116.
- Sun, X., May, S. M., Amelung, W., Tang, N., Brill, D., Arenas, F., Contreras, D., Fuentes, B., Bol, R., & Klumpp, E. (2023). Water-dispersible colloids distribution along an alluvial fan transect in hyper-arid Atacama Desert. *Geoderma*, 438, 116650.
- Tamburini, F., Bernasconi, S. M., Angert, A., Weiner, T., & Frossard, E. (2010). A method for the analysis of the $\delta^{18}\text{O}$ of inorganic phosphate extracted from soils with HCl. *European Journal of Soil Science*, 61, 1025–1032.
- Tamburini, F., Pfahler, V., Bünemann, E. K., Guelland, K., Bernasconi, S. M., & Frossard, E. (2012). Oxygen isotopes unravel the role of microorganisms in phosphate cycling in soils. *Environmental Science & Technology*, 46, 5956–5962.
- Tiessen, H., & Moir, J. (1993). Characterization of available P by sequential extraction. In M. R. Carter & E. G. Gregorich (Eds.), *Soil sampling and methods of analysis* (pp. 75–86). Lewis Publisher.
- Turner, B. L., & Condrón, L. M. (2013). Pedogenesis, nutrient dynamics, and ecosystem development: The legacy of T.W. Walker and J.K. Syers. *Plant and Soil*, 367, 1–10.
- United States Geological Survey (USGS). (2014). *Shuttle radar topography mission (SRTM) 1 arc-second global*. USGS EROS archive. <https://doi.org/10.5066/F7PR7TFF>
- Vet, R., Artz, R. S., Carou, S., Shaw, M., Ro, C., Aas, W., Baker, A., Bowersox, V. C., Dentener, F., Glay-Lacaux, C., Hou, A., Pienaar, J. J., Gillett, R., Forti, M. C., Gromov, S., Hara, H., Khodzher, T., Mahowald, N. M., Nickovic, S., ... Reid, N. W. (2014). A global assessment of precipitation chemistry and deposition of sulfur, nitrogen, sea salt, base cations, organic acids, acidity and pH, and phosphorus. *Atmospheric Environment*, 93, 3–100.
- Vitousek, P. M., & Chadwick, O. A. (2013). Pedogenic thresholds and soil process domains in basalt-derived soils. *Ecosystems*, 16, 1379–1395.
- Vitousek, P. M., Dixon, J. L., & Chadwick, O. A. (2016). Parent material and pedogenic thresholds: Observations and a simple model. *Biogeochemistry*, 130, 147–157.
- Voigt, C., Klipsch, W., Herwardt, D., Chong, G., & Staubwasser, M. (2020). The spatial distribution of soluble salts in the surface soil of the Atacama Desert and their relationship to hyperaridity. *Global and Planetary Change*, 184, 103077.
- Walk, J., Bartz, M., Stauch, G., Binnie, A., Brückner, H., & Lehmkuhl, F. (2022). Weathering under coastal hyperaridity—Late Quaternary development of spectral, textural, and gravelometric alluvial fan surface characteristics. *Quaternary Science Reviews*, 277, 107339. <https://doi.org/10.1016/j.quascirev.2021.107339>
- Walk, J., Schulte, P., Bartz, M., Binnie, A., Kehl, M., Mörchen, R., Sun, X., Stauch, G., Tittmann, C., Bol, R., Brückner, H., & Lehmkuhl, F. (2023). Pedogenesis at the coastal arid-hyperarid transition deduced from a Late Quaternary chronosequence at Papos, Atacama Desert. *Catena*, 228, 107171.
- Walk, J., Stauch, G., Reyers, M., Vásquez, P., Sepúlveda, F. A., Bartz, M., Hoffmeister, D., Brückner, H., & Lehmkuhl, F. (2020). Gradients in climate, geology, and topography affecting coastal alluvial fan morphodynamics in hyperarid regions—The Atacama perspective. *Global and Planetary Change*, 185, 102994.
- Walker, T. W., & Syers, J. K. (1976). The fate of phosphorus during pedogenesis. *Geoderma*, 15, 1–19.
- Walton, C. R., Ewens, S., Coates, J. D., Blake, R. E., Planavsky, N. J., Reinhard, C., Ju, P., Hao, J., & Pasek, M. A. (2023). Phosphorus availability on the early Earth and the impacts of life. *Nature Geoscience*, 16, 399–409.
- Wang, F., Michalski, G., Luo, H., & Caffee, M. (2017). Role of biological soil crusts in affecting soil evolution and salt geochemistry in hyper-arid Atacama Desert, Chile. *Geoderma*, 307, 54–64.
- Wang, F., Michalski, G., Seo, J., & Ge, W. (2014). Geochemical, isotopic, and mineralogical constraints on atmospheric deposition in the hyper-arid Atacama Desert, Chile. *Geochimica et Cosmochimica Acta*, 135, 29–48.
- Wang, L., Jiao, W., Macbean, N., Rulli, M. C., Manzoni, S., Vico, G., & D'Odorico, P. (2022). Dryland productivity under a changing climate. *Nature Climate Change*, 12, 981–994.
- Wang, Y., Bauke, S. L., Sperber, C. V., Tamburini, F., Guigue, J., Winkler, P., Kaiser, K., Honermeier, B., & Amelung, W. (2021). Soil phosphorus cycling is modified by carbon and nitrogen fertilization in a long-term field experiment. *Journal of Plant Nutrition and Soil Science*, 184(2), 282–293.
- Wang, Y., Moradi, G., Klumpp, E., Sperber, C. V., Tamburini, F., Ritter, B., Fuentes, B., Amelung, W., & Bol, R. (2021). Phosphate oxygen isotope fingerprints of past biological activity in the Atacama Desert. *Geochimica et Cosmochimica Acta*, 311, 1–11.

- Weihrauch, C., & Opp, C. (2018). Ecologically relevant phosphorus pools in soils and their dynamics: The story so far. *Geoderma*, 325, 183–194.
- Wilson, S. G., Dahlgren, R. A., Margenot, A. J., Rasmussen, C., & O'Geen, A. T. (2022). Expanding the paradigm: The influence of climate and lithology on soil phosphorus. *Geoderma*, 421, 115809.
- Zhang, J., Feng, Y., Maestre, F. T., Berdugo, M., Wang, J., Coleine, C., Sáez-Sandino, T., García-Velázquez, L., Singh, B. K., & Delgado-Baquerizo, M. (2023). Water availability creates global thresholds in multidimensional soil biodiversity and functions. *Nature Ecology & Evolution*, 7, 1002–1011.
- Zheng, J., Peng, C., Li, H., Li, S., Huang, S., Hu, Y., Zhang, J., & Li, D. (2018). The role of non-rainfall water on physiological activation in desert biological soil crusts. *Journal of Hydrology*, 556, 790–799. <https://www.sciencedirect.com/science/article/pii/S0022169417308211>
- Zomer, R. J., Xu, J., & Trabucco, A. (2022). Version 3 of the Global Aridity Index and potential evapotranspiration database. *Scientific Data*, 9, 409. <https://doi.org/10.1038/s41597-022-01493-1>

SUPPORTING INFORMATION

Additional supporting information can be found online in the Supporting Information section at the end of this article.

How to cite this article: Sun, X., Amelung, W., Klumpp, E., Walk, J., Mörchen, R., Böhm, C., Moradi, G., May, S. M., Tamburini, F., Wang, Y., & Bol, R. (2023). Fog controls biological cycling of soil phosphorus in the Coastal Cordillera of the Atacama Desert. *Global Change Biology*, 30, e17068. <https://doi.org/10.1111/gcb.17068>